NASA/TM–20230003987

Tsunami Early-Warning CubeSat Design Reference Mission (DRM)

Global constellation for near real-time detection, characterization, and warning of dangerous tsunami; detection and evaluation of large earthquakes and volcanic eruptions; and study and continuous monitoring of the ionosphere and climate change.

Oscar L. Colombo and Michael J. Croteau

March 2023

NASA STI Program ... in Profile

Since its founding, NASA has been dedicated to the advancement of aeronautics and space science. The NASA scientific and technical information (STI) program plays a key part in helping NASA maintain this important role.

The NASA STI program operates under the auspices of the Agency Chief Information Officer. It collects, organizes, provides for archiving, and disseminates NASA's STI. The NASA STI program provides access to the NTRS Registered and its public interface, the NASA Technical Reports Server, thus providing one of the largest collections of aeronautical and space science STI in the world. Results are published in both non-NASA channels and by NASA in the NASA STI Report Series, which includes the following report types:

- TECHNICAL PUBLICATION. Reports of completed research or a major significant phase of research that present the results of NASA Programs and include extensive data or theoretical analysis. Includes compila-tions of significant scientific and technical data and information deemed to be of continuing reference value. NASA counter-part of peer-reviewed formal professional papers but has less stringent limitations on manuscript length and extent of graphic presentations.

- TECHNICAL MEMORANDUM. Scientific and technical findings that are preliminary or of specialized interest, e.g., quick release reports, working papers, and bibliographies that contain minimal annotation. Does not contain extensive analysis.

- CONTRACTOR REPORT. Scientific and technical findings by NASA-sponsored contractors and grantees.

- CONFERENCE PUBLICATION. Collected papers from scientific and technical conferences, symposia, seminars, or other meetings sponsored or co-sponsored by NASA.

- SPECIAL PUBLICATION. Scientific, technical, or historical information from NASA programs, projects, and missions, often concerned with subjects having substantial public interest.

- TECHNICAL TRANSLATION. English-language translations of foreign scientific and technical material pertinent to NASA's mission.

Specialized services also include organizing and publishing research results, distributing specialized research announcements and feeds, providing information desk and personal search support, and enabling data exchange services.

For more information about the NASA STI program, see the following:

- Access the NASA STI program home page at http://www.sti.nasa.gov

- E-mail your question to help@sti.nasa.gov

- Phone the NASA STI Information Desk at 757-864-9658

- Write to:
  NASA STI Information Desk
  Mail Stop 148
  NASA Langley Research Center Hampton, VA 23681-2199

NASA/TM–20230003987

Tsunami Early-Warning CubeSat Design Reference Mission (DRM)

Global constellation for near real-time detection, characterization, and warning of dangerous tsunami; detection and evaluation of large earthquakes and volcanic eruptions; and study and continuous monitoring of the ionosphere and climate change.

Oscar L. Colombo
Science Systems and Applications, Inc., Lanham, MD

Michael J. Croteau
Goddard Space Flight Center, Greenbelt, MD

National Aeronautics and
Space Administration

Goddard Space Flight Center
Greenbelt, Maryland 20771

March 2023

Level of Review: This material has been technically reviewed by technical management.

Tsunami Early-Warning CubeSat Design Reference Mission (DRM)

Global constellation for near real-time detection, characterization, and warning of dangerous tsunami; detection and evaluation of large earthquakes and volcanic eruptions; and study and continuous monitoring of the ionosphere and climate change.

Oscar L. Colombo[1,2] and Michael J. Croteau[1]
1. NASA Goddard Space Flight Center
2. Science Systems and Applications, Inc.

March 24, 2023

Table of Contents

Executive Summary

Preamble

This is a report on work performed as part of an IRAD project to study the possible use of a constellation of small satellites such as CubeSats to detect and predict the arrival of tsunami at coastal areas and warn in a timely and reliable way the populations at risk, in order to save lives. The CubeSats would make this possible by providing data from GNSS-R reflectometric receivers they shall carry on board, that can use reflected GNSS signals from the surface below as a form of altimetry. These receivers can also be used to observe ionospheric disturbances below the CubeSats. These downward-focused receivers are in addition to the usual on-board zenith-pointing GNSS navigation receivers for determining the location and clock error of each CubeSat, as well as obtain information on the ionosphere useful to the detection and monitoring of tsunami and other hazards that leave their imprint on the ionosphere above the CubeSats. For example, the proposed constellation also can be used to monitor and quickly determine the seriousness of other natural hazards of similar signatures on oceans and atmosphere, such as large earthquakes and explosive events the like of the Hunga *Tonga*-Hunga Ha'apai volcano in January 2022.

The reflected signals of GNSS (Global Navigation Satellite Systems, presently GPS, GALILEO, Beidou, or GLONASS) are to be used as *signals of opportunity*. Other signals of opportunity that might be used in reflectometry (e.g. from communication satellites) have been considered and reported in the technical literature, but using those from GNSS satellites is now common practice with a very considerable body of published work, so they are the signals considered in what follows.

The proposed mission: Motivation, technical means and objectives:

The main thrust of this study has been in finding out how such a constellation could be useful for detecting and monitoring such natural hazards as: tsunami, earthquakes, volcanic explosions, and big storms at sea (hurricanes, cyclones, typhoons). As part of this study, we have also investigated the possible use of the same data to monitor the effect and progression of global climate change by registering information of the level of rivers and lakes, the humidity in the soil, the biomass in forested areas, and the winds on the sea surface and corresponding sea state. All these variables are already monitored by present day smaller satellite constellations, including CubeSat ones dedicated to these types of observations, something that may be significantly augmented with a faster whole-world coverage by the constellation studied here, with some 360 CubeSats at, as also chosen here, 550 or 600 km altitude, with polar or near-polar inclination, in eight equispaced orbit planes. The number of satellites and of planes was chosen to ensure a dense coverage of almost the whole world in every orbital period of 95.3 or 96.5 minutes, respectively, common to all satellites in this constellation depending on their chosen altitude. CubeSats will pass near enough to observe closely multiple times the same 1 degree x 1 degree area on Earth approximately every two minutes.

This report covers the following topics:

1) The proposed constellation of CubeSats, its likely geographic data coverage, and possible ways to deploy it.

2) The GNSS-R receiver.

3) Reflectometry:
Specular-point tracks and ellipses of constant signal delay with hyperbolas of constant Doppler shift are used to find vertical profiles of tsunami waves along the tracks and 3-D Delay Doppler Maps (DDM), both very useful for detecting and tracking in real time as well for studying tsunami, wave propagation, etc., offline.

4) Detection of tsunami.

5) Detection of large earthquake and volcanic activity.

6) GNSS-R as a tool for monitoring global climate change.

7) Data transmission.

8) The possible use of Spire GNSS-R data in an extension to this project.

9) Issues to investigate further, including simulations.

10) Summary and conclusions.

Main points explained in some detail:

In the case of tsunami, how to find them and to determine their size, direction, and velocity at successive epochs is the main application of reflectometry studied in detail in this first stage of this IRAD study. Such information can help make more reliable predictions of the tsunami future progress and, based on these predictions, issue more reliable advanced warnings about where, when, and with what effect the tsunami may pose a threat to coastal populations. The information about tsunami from the CubeSat constellation would be combined with data from other sensors already deployed to this effect, such as the networks of sea-floor pressure tide gauges mainly deployed along some continental margins and some scattered across the high seas. If possible, private companies operating CubeSats of their own could work cooperatively with such a mission to enhance or add different aspects of it with their own data and expertise, or as contractors doing parts of the actual work needed.

These objectives should fit within current activities at NASA, for example:
NASA's Space Geodesy Project already supports tsunami risk reduction through collaborations with the International GNSS Service, which manages the GNSS-enhanced Tsunami Early Warning Systems (GTEWS), the International Association of Geodesy's Global Geodetic Observing System (GGOS), and the Group on Earth Observations (GEO) Geodesy for the Sendai Framework Community Activity.

For earthquakes and volcanic explosions, the reflected and direct receiver data would help detect the effect of atmospheric gravity and acoustic waves generated by these hazards. These are waves that propagate upwards through the troposphere and then the ionosphere and can be mapped by combining the data from the navigation and GNSS-R receivers. By processing the multiple frequency signals transmitted from the GNSS satellites with both receivers, it is possible to estimate the total free-electron content above each LEO and between it and the transmitter in each GNSS satellite tracked. With the reflected signals captured by the GNSS-R receiver, one can additionally estimate the electron content below, together mapping the whole ionosphere. Besides this contributing to the study of the ionosphere and its interactions with both terrestrial and space weather events (such as solar coronal mass ejections and the effects that these have in the tropics and the aurora intensity in polar regions) the mapping of the ionosphere should show, for example, a distinct signature of global climate change: an actual cooling due to the trapping of Earth's re-radiated heat in the lower atmosphere by greenhouse gases, heat that no longer will reach it at its otherwise faster rate.

There are three main ways of realizing the stated purpose of the CubeSat constellation to be explained in the main part of this report:

1. The sea surface height profiles obtained along the tracks on the sea surface of the specular points, the brightest parts of the reflected signals of the GNSS satellites tracked by a LEO, and how these can be used to determine the shape, speed, and direction of tsunami waves. These points move at a velocity of several km/s across the sea surface, that is one order of magnitude faster than the fastest tsunami.

2. The Delay Doppler Map (DDM): as explained in the corresponding paragraphs, what is this, how is it made and hardware requirements depending on the type of receiver. Applications of the DDM are possible and implemented and are used to study such things as: sea state (waves), ocean surface wind velocity in large storms, soil moisture in agricultural areas (particularly those affected by drought), sea ice (the extent of ocean it covers and its characteristics), snow depth in polar regions, and more, all of which are relevant to monitoring climate change.

3. The effect on GNSS signals of the free-electron density waves in the ionosphere generated by the tsunami, earthquakes, and violent explosions.

An issue preliminarily investigated here and the natural object of in-depth future research, is the way the data will be analyzed. A review of the relevant published work suggests that the method known as the Ensemble Kalman Filter is a likely candidate. This is a data-driven technique, widely used to estimate corrections to complex dynamic models such as those developed for the oceans and ionosphere, with state vectors of perhaps millions of error-state components. The calculation probably would be possible only using supercomputers on the ground, so the transmission of the necessary data from CubeSats to the analysis center on the ground is an issue also studied here in considerable detail.

4) Detection of tsunami (and present motivation):

Figure i and the video at the following link give an idea of the magnitude of the potential catastrophe due to a tsunami, and gives an indication of what motivates the work reported here: https://education.nationalgeographic.org/resource/tohoku-earthquake-and-tsunami

The detection of tsunami must be made in real time and transmitted to the ground processing facility via satellite links, possibly via commercial satellite telephony. In this respect this is different from the way data to be used offline is downloaded.

(Note: depending on software used, to read or watch the URL linked articles or videos, then return to this document, it is best to do so while viewing this document **not** in full-screen view.)

Figure i: Arrival of the tsunami of March 11, 2011 caused by the magnitude 9 Tohoku earthquake at sea to a coastal town in Japan. (Photo: Reuters; http://archive.boston.com/bigpicture/2011/03/massive_earthquake_hits_japan.html)

The reflected signals from the sea surface, at present, have an observation noise larger that the height of most tsunami in open waters, except when the surface grazing angles of the reflected signals are quite low, something that limits the precise data available to those from reflections occurring at long distances from a CubeSat subsatellite point. However, possible ways to improve on this, particularly for doing better GNSS-R altimetry, are likely to be tested in coming years. *More importantly: a tsunami is like nothing else that can be observed in the oceans: it is a*

series of waves of hundreds of km wavelength, traveling at the speed of a fast propeller airplane, from 100 to 200 hundred meters per second. These remain the same for considerable periods of time, for as long as the depth of water does not change significantly, for example across much of vast ocean basins. All these characteristics are well known and understood and suggest possible ways of taking advantage of them to detect tsunami and filter out regular wind waves and data noise to get a clearer view of them and predict their progress. This shall be the central topic of future work on this matter.

Damage caused in the USA by the March 2011 Tohoku-oki tsunami:

The arrival of the tsunami to the shores of the inhabited islands of Hawai'i and California caused serious damage and at least one death:

- Hawaii:
  https://dod.hawaii.gov/hiema/files/2021/03/2011-Hawaii-Tsunami-10-Year-Anniversary.pdf

- California:
  https://www.conservation.ca.gov/cgs/tsunami/tohoku

Several large tsunami directly or indirectly triggered by large magnitude earthquakes have occurred since the late 1940's through recently in the 21st Century and are described here:

https://sos.noaa.gov/catalog/datasets/tsunami-historical-series-aleutian-islands-1946/

The 2004 Boxing Day (26thDecember) Indian Ocean Tsunami:

One of the most lethal in history, with some 168,000 dead or missing in Indonesia and 60,000 mores in all the inhabited coasts and islands of the Indian Ocean:

https://en.wikipedia.org/wiki/2004_Indian_Ocean_earthquake_and_tsunami

Sensor:

The necessary data shall be obtained with a GNSS-R receiver in each CubeSat consisting of both a dual-frequency navigation receiver and a reflectometric receiver. The navigation one will, based on the distance to the GNSS satellites being tracked, determine the precise satellite position and velocity at every epoch, as well as the precise time when the observations were transmitted and then received. The data from reflectometric receiver, used to find the delays and Doppler shifts of the reflected signals from the surface below, will be, in the case of tsunami, used in near-real time to monitor the natural hazard progress across the ocean and amplitude of the wave front and issue warnings when necessary, while it will be used off-line for finding and mapping sea storms and studying the condition of other types of surface: land, ice, snow, deserts, forests, prairies, etc.

The navigation receiver data are also to be employed for sensing the atmospheric disturbance produced by the passing of a tsunami, as this disturbance propagates upwards as gravity waves in

the thinning air leaving behind a regular ascending wave-like pattern on the dispersive free-electron content. This content delays the received signals to an extent that depends on the signals' frequencies. So this electron density can be estimated from the difference in the delays of signals of different frequencies. The electron content so obtained can be used to map in three-dimensions the electron density above the CubeSats, with enough signals from satellites crisscrossing the ionosphere in different directions (ionospheric tomography).

The reflectometric data can be used to map those waves in the ionosphere below the CubeSats, as well as to obtain the sea height above an appropriate reference surface: the difference between reference and true surface along the path of the specular point of each GNSS satellite in view from a receiver. These points move close to the horizontal speed as the CubeSats, following tracks roughly parallel to its ground track, because the angular orbital speed of the CubeSat, with an approximate period of 95 -97 minutes, depending on the chosen altitude, is some 7.6 times higher than that of the GNSS satellites, with a period of 720 minutes, and surface speed is proportional to the angular speed times the Earth's radius. The resulting vertical profiles should show the vertical outline of the tsunami wave that, unlike the errors in the reference surface, will move at a very high speed that is always a large fraction of the speed of sound at sea level. This makes possible their identification and the determination of their direction, speed, size and shape along the specular point tracks, and these results can later be refined further as explained in this section.

Several errors in the data must be corrected: the errors in the clocks of the GNSS satellites (previous standard relativity correction to the GNSS clock time, to put these and the receiver clock, virtually, in the same timeline, at the same height above the geoid so they all run at the same apparent clock rate); the effect of the refraction due to water vapor in the troposphere as well as to atmospheric pressure; the ambiguity in the carrier phase measurements; and the effect of tides, both ocean and solid Earth, and of the loading effect of these on the Earth crust. Some of these calculations need not be made at the CubeSats but would better be done at a terrestrial processing center with adequately powerful computers and the necessary software, using the data received from the constellation. (Depending on the progress made on the already being developed more powerful computers that can be used in CubeSats.)

5) Large earthquake and volcanic activity detection.

These natural hazards are violent enough to produce direct effects on the ionosphere that can be used to detect their occurrence and follow their development by observing the free-electron density waves radiating upwards and horizontally from a point above and nearby where the event has happened.
Techniques that can be used to analyze the ionospheric signatures of tsunami can be used with the same purpose here.

6) GNSS-R as a tool for Monitoring Climate Change.

Over more than two decades, various aspects of Climate Change have been observed from space and small satellites equipped with GNSS-R receivers have proven increasingly useful for this.

Among other applications, CubeSats have been used to study sea winds, cryospheric ice and snow cover, soil humidity, status of wetlands, vegetation cover and its status, etc.

7) Data transmission.

Because the information that must be transmitted in real time to the ground processing center that is part of the tsunami detection effort must be sent at a rate compatible with the communications bandwidth available, the data will have to be compressed **losslessly**. This is explained in the section on Communications.

The likely means for transmitting data in real time include the use of satellite telephony systems that can provide the required bandwidth, for example some of the services available to users of the Iridium constellation.

8) The possible uses of Spire GNSS-R data.

Spire, a company based in San Francisco that has developed its own constellation of CubeSats for remote sensing of weather and is now beginning to do GNSS-R work as well, has a contract with NASA to provide it with both raw data that can be used to test ideas on how to extract information relevant to the purposes of the mission under study and also products obtained processing those data that can be used to validate the results obtained when testing those ideas, collected with their CubeSat constellation STRATOS receivers that are used for two complementary types remote sensing:

1. Radio Occultations, for mapping vertical profiles of the troposphere's water vapor and the ionosphere free-electron content density, temperature and other variables of interest in meteorology, and for monitoring space weather, scintillation and other processes of value in radio communications, reliable GNSS satellite positioning, as well as various other matters of engineering and scientific interest.

2. A new generation of STRATOS receiver, used originally as a sensor dedicated to radio occultations and ionospheric observations, now also can work as a GNSS-R receiver, providing data relevant to various important aspects of the Earth's surface that are, among other things, indicators of Global Climate Change.

More details about Spire, STRATOS and it's uses can be found here:
https://www.eoportal.org/satellite-missions/spire-global#a-healthy-trend

Spire's is an example of the data and products a constellation of CubeSats is, even today, capable of contributing to aspects of the possible mission studied here, although the Spire constellation is not intended to be continuously available for the near-real time detection and monitoring of tsunami, earthquakes, and volcanic explosions.

The main task of an integrated international cooperative effort has to be one where the diverse and relevant data obtained by each organization involved (e.g., NOAA with its DART system of sea-floor deployed pressure tide gauges, various nations' conventional coastal tide gauge systems, etc.) and including data from commercial companies such as Spire, is pooled and combined. The constellation proposed here could be a major contributor to obtaining quicker and more reliable results.

The capabilities and characteristics of sensors and of CubeSat's other hardware, such as that used at Spire, can be helpful as examples of the design and selection of the equipment to be used in the proposed constellation. Companies such as Spire may also contribute their valuable experience, additional data and processing services.

9) Issues to investigate further, some using simulations.

The analysis of the noisy GNSS-R data, how to improve its precision, and the likely quality of results using various data analysis approaches, by means of simulations of data coverage, assuming different possible data qualities, to be used in covariance error analyses and in other ways to investigate possibly effective methods of processing the data from the assumed eight-orbit plane, 360 CubeSats constellation, with 45 CubeSats in each plane, in near-circular high inclination orbits and at a height between 550 and 600km.

The uses of GNSS-R for monitoring climate change.

The use of hydrodynamical models to both assist in making and also refine the estimates made with GNSS-R data from the CubeSats of tsunami waves shape, direction, and speed. These models could be started and then updated in near-real time with those data being processed with an appropriate recursive Bayesian estimation procedure, such us the Ensemble Kalman Filter. A similar approach using dynamic (physics based) ionospheric models may be possible using both navigation receiver and GNSS-R ionospheric data obtained by differencing GNSS signals of different frequencies.

The possible computer power available for use in CubeSats, including some very powerful computers for use on board, now being developed. The desirable set of CubeSat compatible hardware components and what are the choices currently available. And perhaps also in the future.

Make a preliminary study of Spire data available through NASA to decide how it could best be used in future mission planning as part of a longer-term funded project with a group of experts.

End of Executive Summary

Main Report

A Note on CubeSats:

CubeSats are small satellites; at their smallest they are cubic-shaped, typically of 10 cm each side. These are known as "one unit" or "1U" CubeSats. However, several CubeSats can be joined together to form a longer, rectangular cuboid shaped "CubeSat." Two examples are shown in the Figure below. In figure (a) a basic "cubic" CubeSat. Figure (b) shows two generations of the 3U CubeSat "Lemur" of the Spire company, of which and of its relationship with NASA more shall be said in this report.

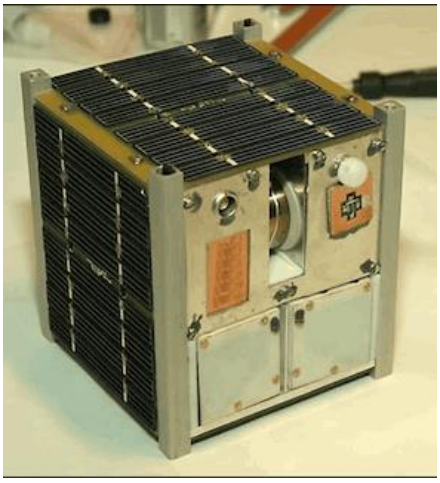

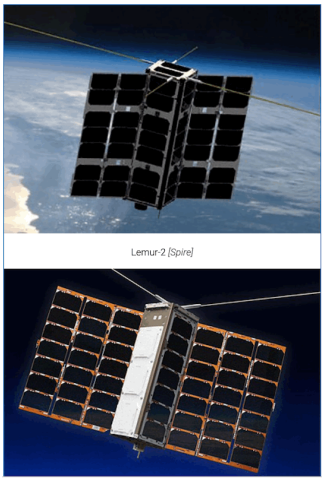

(a) Basic shape, 1 U CubeSat (b) 3-U CubeSats with solar panels.

c) Trends in CubeSat deployment

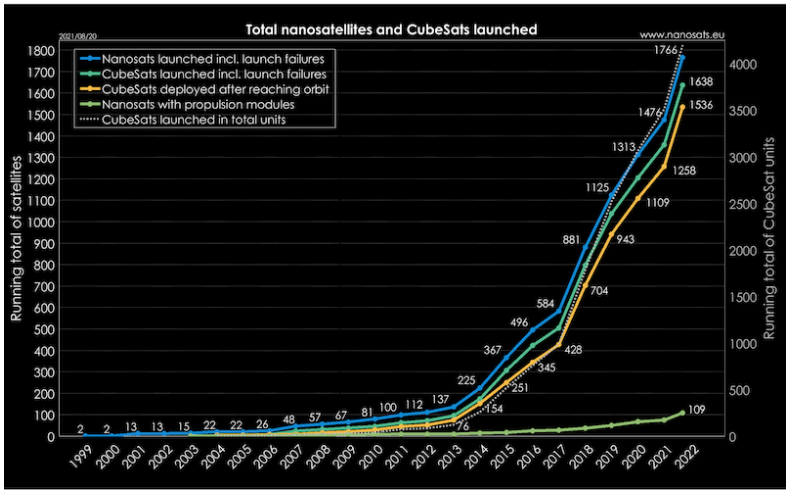

(a) From Wikipedia "CubeSat" article. (b) From Gunter's Space Page https://space.skyrocket.de/doc_sdat/lemur-2.htm

(c) https://commons.wikimedia.org/wiki/Category:CubeSat_satellites#/media/File:Total-CubeSats-Launched.png

1) The Proposed Constellation.

Each one of the more recent LEMUR-2 satellites, such as those in Figure (b), is a 3U CubeSat 10x10x34.5 cm in size, being designed, built, and operated in-house by Spire. Less than 6kg in weight, the LEMUR is powered by a deployable solar array and by solar cells also on their bodies. They remain orbit at 400-650 km altitude for about 2 years.

More generally, CubeSats may carry a variety of sensors and equipment comparable in kind, if often not in dimensions, weight, or power consumption, to those in full-size satellites. For example, the Spire Lemur-2 2nd generation CubeSats feature, besides the GNSS, GNSS-R and GNSS-RO (for occultations) receivers and corresponding antennas, full 3-axis attitude control systems, while RF communications are provided via UHF and S-band. For more details, see https://en.wikipedia.org/wiki/CubeSat.

CubeSats may also carry some means of self-propulsion for station keeping and other maneuvering in the form of small, low-power cold gas, chemical or ion thrusters as well as experimental solar sails. Many components are Commercial Off The Shelf (COTS) and some are custom-built or specially designed for use under the power, size and weight limitations typical of CubeSats.

Orbits, orbital planes, deployment of CubeSats on their orbits in each plane:

After considering several possible arrangements, a good one from the point of view of near complete coverage with the obtained data of the Earth's surface is likely to be one with several orbit planes, the orbits ascending nodes distributed at constant intervals along the equator and an equal number of satellites in each, in near-circular orbits and with a high inclination to ensure extensive Earth coverage. The satellites in each plane could include a few spare ones evenly distributed between groups of as many active CubeSats as the number of spares in each plane. As an example, the surface coverage of such a constellation during the time of one complete revolution of all the CubeSats in it is shown in Figure 1.

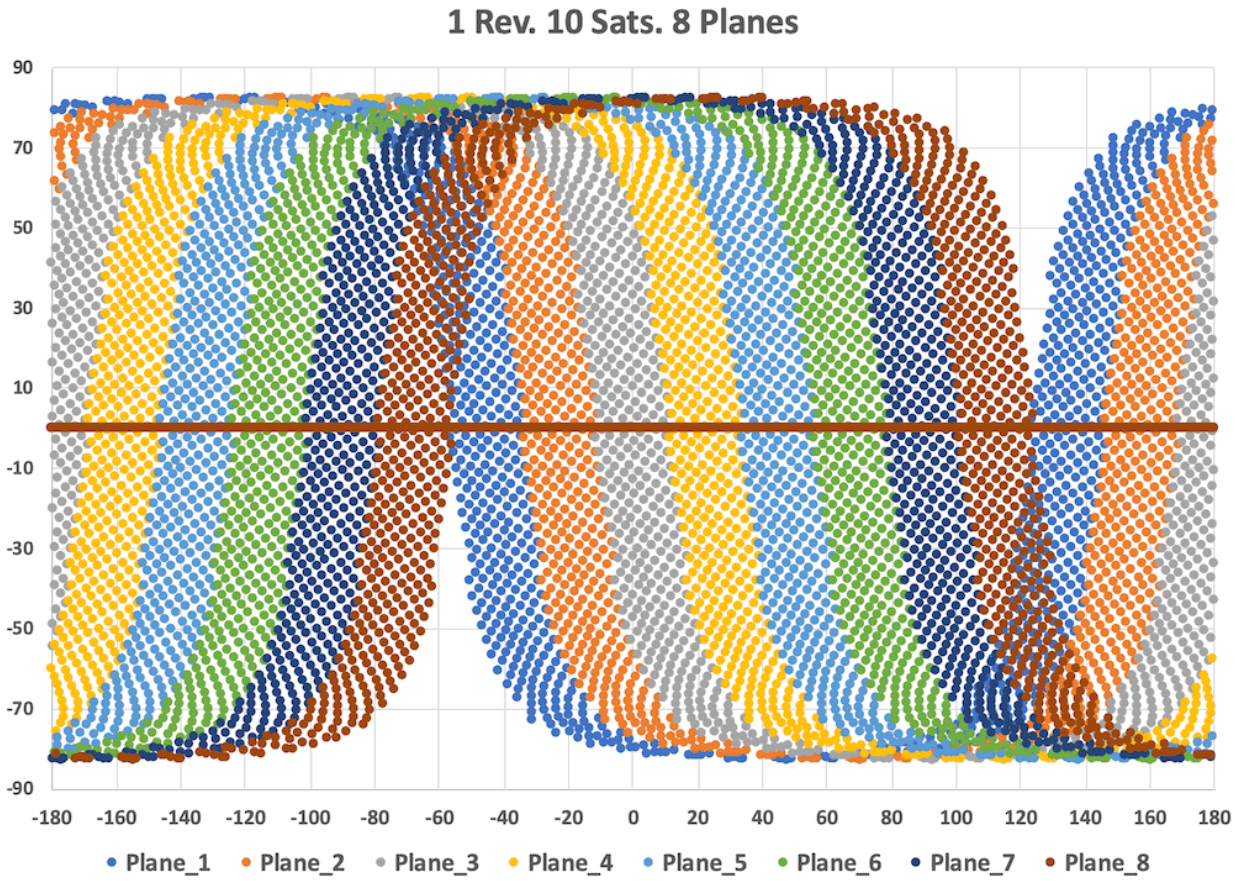

Figure 1: An example of the Earth's surface coverage in one revolution (some 95 minutes at 550 km altitude) of every satellite, for a constellation with 8 planes each with 10 satellites at an inclination of 98 degrees.

With more satellites in each plane, this picture will not change in the extent of the Earth surface covered, it merely will become denser, something desirable, given the objectives of the proposed mission, with more points inside the color bands shown here. The proposed constellation will have some 45 satellites per plane.

Notice that this coverage is repeated at every orbital revolution of the whole constellation, only shifted towards the West by some 22.5 degrees in longitude from the previous one after each revolution, due to Earth's rotation. The parts left uncovered are greatly exaggerated in this figure by the rectangular projection used. The ascending and descending nodes of each pair of planes could be together, the planes sharing a common line of nodes as, for example, in the GPS constellation, or be opposite to each other relative to the geocenter, so the lines of nodes are not shared by pairs of planes. The separation between consecutive nodes would be twice with shared lines of nodes that without, so the latter is preferred, as it makes for a greater overlap of the areas in view by satellites in neighboring planes, the further from the equator where this overlap is at its minimum.

A different launch could be made for the CubeSats of each plane, or a parking orbit approach needing a single launch could be used, or a combination of both. All the satellites will have the same altitude, chosen to be somewhere between 550 and 600 km, and in near-circular orbits. The reason or choosing these altitudes is to ensure that atmospheric drag won't deorbit the satellites too quickly. The expected useful life of a satellite can be limited by a number of different factors, but as far as air drag goes, that depends mainly on the product of: air density x CD x area/mass ratio, where "area" is that exposed, on average, to the incoming air and CD is an aerodynamic coefficient that depends on the roughness of this surface and on its shape. The air density may be very small, but it can vary considerably over a solar cycle as well as during geomagnetic storms, especially severe ones caused by the direct, or even just glancing, impact of a Sun's coronal mass ejection. At those altitudes the air drag is low enough for the satellites, designed to have a sufficiently low area to mass ratio, to stay in orbit for several years before drag, or some self-propulsion means commanded from the control center, deorbits them.

For maximum coverage of the oceans, and of the Earth for studying global climate change, the orbits could be all polar or sun-synchronous, particularly if the CubeSats also carried cameras on board. There could be other advantages as well in choosing sun-synchronous, which are slightly retrograde. At some 98 degrees inclination, ground-track coverage with such orbits is almost complete except for two small circular regions around the poles. But the areas observed from all CubeSats there overlap.

Choice of the constellation example:

As already indicated, the constellation in Figure 1 has eight planes with equally spaced ascending and descending nodes around the equator. These orbital planes have their nodes at the corners of a regular 16-sides polygon (hexadecagon) with twice as many vertices than the number of planes and with all the ascending nodes on half the equator and the descending ones on the other half, the lines of nodes being the diagonals of the polygon. As mentioned earlier, the planes so chosen do not share their lines of nodes in pairs, thus the separation between planes is half the angle at the equator than it would be if the lines of nodes were shared by pairs of orbit planes. This shorter separation allows for a greater overlap of the areas observed from satellites in adjacent planes and, consequently with more data being collected in the area observable from any of the satellites. The smallest overlaps will occur at the equator, where the distance between consecutive planes is greatest. The overlaps increase as the orbits converge towards the poles. Even at the equator, with such an arrangement, the satellites at each adjacent plane would cover, from either 550 km or 600 km heights, as much or more of the "left" and the "right" half of the area that can be observed by the satellites in the middle plane, potentially doubling the number of observations in this area. The minimum number of planes with these properties that allows for such an overlap at the equator is eight. Seven would not be enough, leaving larger poorly observed or unobserved areas at every 96-minute revolution, particularly in the tropics. Nine planes would be more than strictly necessary, which is an important consideration, as frugality of resources to achieve a given end is a desirable design attribute, particularly when it comes to space missions.

Of course, many different configurations of a CubeSat constellation are possible, each with their comparative advantages and disadvantages, but only one could, in the time available for this study, be considered in sufficient detail and the one in Fig. 1 was the one.

Constellation deployment:

The deployment of the satellites in orbit could be made directly to each plane with a single launch exclusively for it, or to a parking orbit. Both methods are often used. In each case the satellites will be packed inside a container or pallet, this with its own propulsion engine to move along the intended common orbit on that plane, with a slightly different orbit parameters than the chosen ones for the CubeSats. This way, the container drifts along, deploying the CubeSats, one at the time in their intended locations on their common orbit, as it goes by these locations. While there could be a single such pallet for the case of one launch directly to each orbit plane, if a parking orbit is used exclusively instead, there will be, at a minimum, as many as the number of planes.

In the parking orbit approach and with the CubeSats at some 550 or 600 km altitude, the parking orbit has to have a considerably different altitude, for example 800 km. This is because these pallets must stay in orbit for the whole duration of the deployment process, which at that altitude and inclination can take close to two years, and if chosen significantly lower than the CubeSats would probably not remain in orbit long enough for that, because of the greater air drag than at those higher altitudes. The parking orbit, being sufficiently higher than the final orbits, will drift under the influence of the Earth's equatorial bulge at a slower rate than the planes of the CubeSat ones. This is because the plane drift rate is proportional to both the ratio of the square of the Earth radius to the square of the distance of the satellite to the Earth's center, or geocenter, and to the cosine of the orbit inclination. And because of it being also proportional to the cosine of the inclination that, in the orbits considered here, is close to 90, the drift rates of both orbits, and therefore their relative drift, which is what matters here, are quite slow. More precisely, ignoring a small term in the eccentricity e, as the orbits are near-circular, with negligible e:

$$\omega_p = -3/2\ J_2\ (R_e/a)^2\ \omega\ \cos i$$

where:

ω_p is the node precession rate (in rad/s),
R_e is the body's equatorial radius (6378137 m for Earth),
a is the semi-major axis of the satellite's orbit,
ω is the angular velocity of the satellite's motion (2π radians divided by its period in seconds),
i is its inclination,
J_2 is the 2nd (and largest) zonal of the geopotential, from the Earth's oblateness, ~ 10^{-3}

Soon after the vehicle bringing the pallets enters the parking orbit and releases them, one will make a small delta V of some meters per second and go down to the intended orbital altitude of the first plane and settle in an orbit there slightly higher or lower than the intended altitude of the CubeSats, so it will drift along it at a slightly different velocity deploying these in their common orbit, as already mentioned. The pallet may remain in its orbit, drifting along, so it can be used to move a spare satellite to fill a gap caused by a malfunctioning CubeSat. This is a question that needs to be studied in detail when planning the actual mission, to decide if this is a practical idea.

It might be better simply to fully activate the replacement satellite in its current position within the common orbit.

Once the satellites are in their correct places in their lower nominal orbit, but still in the plane of the parking orbit, the plane of both parking and the CubeSat's orbit drift from each other, as they turn under the influence of the bulge at different but always slow rates about the Earth's axis. This rate is less for the higher parking orbit because it is farther away from the bulge and its gravitational pull is consequently less. Eventually this relative drift will position the parking orbit plane as far from the first as the planned difference between the ascending nodes of two consecutive orbit planes. Then a second pallet goes down and deploys the CubeSats of the second plane in their orbits there, and so it continues until all the planes have been populated with their CubeSats.

The higher the parking orbit and the lower the CubeSats one, the higher the relative drift rate of the lower CubeSat one and the shorter the time it takes to deploy the constellation. Regardless of the choice of orbits, the whole process takes a long time: With six planes, from 2.8 to 2.2 years with the parking orbit at 800 km and the CubeSats common orbit at 600.0 km and 550 km of altitude respectively. With 8 planes, it will take 2.9 to 2.3 years. Either way, it will take a significant part of the expected lives of the satellites under the harsh conditions of space, hard radiation in particular.

The above assumes that the orbit planes inclination is 98 degrees, so the orbits are not quite polar, but sun-synchronous. Polar orbit nodes do not drift, so the parking orbit approach is not applicable to them. Orbits with an inclination of less than 90 degrees, being prograde, will drift in the opposite direction of the retrograde sun-synchronous one considered here.

To quicken things up while reducing the number of launches to less than the number of planes, a mixed approach with parking orbit deployment for some orbit planes and direct to orbit for the others could be used.

Finally, it must be noted that if pairs of orbit planes share the same line of nodes, with their ascending and descending nodes close to each other, the time to complete deployment with one parking orbit would be twice as long than if the planes had separate ascending and descending nodes equispaced along the equator. With an even number of planes and ascending nodes and descending nodes on the same spots, the ascending nodes lie all around the equator, on the vertices of a regular polygon with as many vertices as planes, while with separate nodes they lie on a polygon with twice the number of vertices as planes and all the ascending ones are within half of the Earth's equator and the descending ones on the other half. The latter configuration has been assumed in this report.

Area observed from a CubeSat from orbit at any given time:

It will be a spherical cap with a radius that depends on the satellite height above the Earth's surface:

Satellite height (km): 550
Distance sub-satellite point to horizon (km) 2558.6
Or in degrees along max. circle: 22.98

Satellite height (km): 600
Distance sub-satellite point to horizon (km) 2664.26
Or in degrees along max. circle: 23.9

Area overlaps of observations from satellites in adjacent and the same planes:

The separation of the consecutive ascending and descending nodes of eight orbit planes with ascending nodes that are not at the same points on the equator as the descending ones, is equal to 360/16 degrees, or 22.5 degrees.
This means that, at the equator and at the altitudes of 550 and 600 km, as shown above, there is considerable overlap between the observations made from successive satellites on the same orbit plane, provided that they are equally spaced along their common orbit, and satellites in adjacent planes will have the tracks of their specular points crossing over about half of the same area surveyed by any in the middle plane. As the quality of the reflectometric data increases with decreasing grazing angle, or elevation angle about the sea surface of the incoming and reflected signals, which happens with increasing distance from the sub-satellite point, the region with less noisy data found away from the satellites on one plane will overlap that with the noisier data around the central sub-satellite points of those in the next plane, providing a rough levelling of the combined strength of their signals across their respective observable regions. The CubeSats' observable areas will overlap further as the orbit planes converge towards the poles, so more data will be collected over increasingly smaller areas and with greater density, the closer to the Poles.

If the number of satellites in each orbit plane is 45, as in the constellation studied here, at 600 km the average separation between satellites in the same plane will be of 963.4 km. At a height of 550 km, it will be 956.4 km. So there will be on average more than five satellites over the same area of roughly 2540 km - 2650 km across that can be observed at once from its center at the given altitude. Their areas of data coverage will overlap, the stronger signal ones with the weaker ones, same as those between satellites in different planes, only that the separation of the positions of these satellites in the same plane will not change with latitude, while that with those in adjacent planes would decrease with it. (In the case of adjacent planes, the useful overlaps need not be between satellites in these planes running parallel to each other at the same time, but at closely time-spaced intervals of a few minutes each.

2) The GNSS-R Receiver.

2.1) The GNSS signals and the Navigation Receiver:

The GNSS satellites transmit their signals in the L band of the frequency spectrum.
The signals' carriers are modulated with a spread-spectrum code of +1, -1 rectangular pulses that is periodical, with a period, or repetition rate, in the case of GPS, of 37 weeks; a coarse acquisition code (or C/A code) with 1 millisecond repetition rate that is used to lock the receiver onto the signals of a particular satellite. In GPS this is a pseudo-random sequence of 1 and -1 rectangular pulses that is unique to each GPS satellite and has a practically zero cross-correlation with those of the other satellites. [1], [2].

The signals and their carrier frequencies of the USA GPS transmissions are:

L1	1575.42 (Of Coarse Acquisition code, not encrypted.)
L1C	1575.42 (Civilian use, not encrypted with the antispoofing code)
L2C	1227.6 (Also for Civilian use, unencrypted)
L1P	1575.42 ("P" for "Precise" code, encrypted with antispoofing)
L2P	1227.6 ("P" for "Precise" code, encrypted with antispoofing)
L5	1176.45

Those of GALILEO (European Union - ESA):

E1	1575.42 (Encrypted, only for approved users with key)
E5a	1176.45
E5b	1207.14
E5	1191.795
E6	1278.75 (Encrypted, only for approved users with key)

Those of Beidou (China):

B1I	1561.098 ("I" stands for "in phase, "Q" for "in quadrature")
B2I	1207.14
B3I	1268.52
B1C	1575.42
B2a	1176.45
B2b	1207.1

(There are five restricted access signals besides the open access ones listed above: B1Q (quadrature), B1a, B2Q, B3Q and B3a)

Those of GLONASS (Russian Federation):

L1 C/A	1598.0625-1609.3125
L2 C	1242.9375-1251.6875
L2 P	1242.9375-1251.6875
L3 OC	1202.025

GLONASS signals are all transmitted in the clear, but some are restricted to only approved civilian users "by obscurity", that is by using secrecy concerning certain characteristics of those signals, which knowledge is necessary for building receivers capable of using them. GLONASS

also has a different way of separating the various satellite signals, known as Frequency Division, where each satellite transmits in a different frequency, while the other three systems, GPS for example, transmit in the same frequencies and are separated by their acquisition codes, or by Code Division. In these three systems the main frequency, that also carries the equivalent GPS C/A (or in the current 3-letter names system, C1C), is the same or nearly the same for each of these three systems. These systems are designed to avoid mutual interference, as a result of agreements between the government responsible for each system. Finally, a coded series of digital data is added as the modulations to the IP component conveying the Navigation Message, such things as the satellite orbit elements that can be used to predict the position of the satellite over, e.g., the next two hours, also corrections for the satellite clock, etc. All these data are needed for the receiver computer to find the position, velocity and corrected time of transmission. The satellite transmits signals in two or more frequencies, three in the case of GPS and 4, 5 and 6 in the case of GLONASS, GALILEO and Beidou, for example.

Selected Availability and Antispoofing encryption of GPS signals:

After the first constellation of GPS satellites, or Block I, was deployed in the early 1980s, being of military purpose and with the Cold War still going on, the precise use of GPS signals was restricted with an encrypted jitter of the satellite clocks that could be corrected only with the appropriate receiver software and knowledge of the encryption key. This was known as "Selected Availability", or S/A for short. The de-encryption key was distributed for use in military receivers and was supposed to be changed often. But this proved hard to keep up by soldiers during actual military operations, particularly in wartime. So during the first Gulf War, in the early 1990's S/A was turned off and the clock signals transmitted "in the clear". This prompted the eventual issuing of a Presidential order to turn S/A to "a minimum level" that was, in reality, zero. And it has stood this way ever since. But already before that, civilian users all over the world were using a technique that defeated it: interferometric or differential GPS. This is still used to some extent and consists in getting data from at least two receivers: one or more "reference" ones and the user's, where the latter can be stationary or in motion, for example on an airplane, and differencing their data, thus removing the clock error of both satellites and reference receivers, because these errors are common to all receivers. And removing also the effect of S/A, as this was an artificially introduced clock error. When the GPS constellation was declared officially operational, an encrypting modulation known as the W Code was added to the Precise code in L1 and L2. This was, in fact a "friend or foe" signal that indicated this was a real GPS satellite-transmitted signal and not a decoy broadcast from an enemy's high-fling airplane hard to detect, or some hidden location and meant to "spoof" the receivers that might lock onto it as if it were the transmission of a real GPS satellite. This encryption is still in place. Using at least two frequencies is essential for either eliminating the effect of the ionosphere, as is the case in most applications, or also for estimating it, as is of interest, for example in the study of the ionosphere and also in monitoring Global Climate Change, as in the applications considered here. Eventually techniques have been developed to make possible to remove the W code without the encryption keys [3]. Because these receivers do not have direct access to the P code in L2, they are also known as "semicodeless receivers." [4], [5]

The result is not as good as using the de-encryption key, but have proven to be good enough for many applications. Years later, in the late nineties, two new civilian signals: C2 (or L2C in the

new naming system) in the L2 frequency similar to C/A code in L1) and L5, similar to the encrypted P1 and P2 signals, were introduced. But there have not been fully supported (C2) or not working well enough (L5) until recently, so they have come into use only recently as of this writing.

Because the process of finding ways to overcome the limitations on the use of GPS without an alternative civilian signal in L2, imposed by Antispoofing, took a long time during which the only alternative to GPS was the Russian GLONASS, with some disadvantages compared to GPS, many GNSS-R receivers were "L1 only", using the C/A code to obtain the delay, Doppler, and phase from the satellite signals.

The W code has a much narrower bandwidth than the P code, and thanks to this it has been possible to remove it, as pointed out here. However, the encrypted signals of GALILEO are much harder to use without their encryption keys, because of the way they are encrypted, but there are enough GALILEO unencrypted ones at different frequencies instead, so encryption does not present an essential problem here for using GALILEO as well as GPS, for example.

Use of GPS L2 signals in CubeSats:

Only quite recently, with the introduction of civilian L5 and C2, has it been practical to make receivers that can be used on CubeSats that are capable of tracking the delay in both L1, as always, and in L2 and L5, so many of the receivers in use on CubeSats are still L1-only receivers. L1 and L2-capable ones started to be used only recently, as well as those capable of tracking other GNSS constellations besides GPS. Because GPS was the first GNSS ever put in operation while, with the exception of GLONASS, those other constellations followed GPS by a number of years and some took a very long time to become operational, or started to be deployed much later than GPS to be considered for regular use until years later, GPS (and to a lesser extent GLONASS) was and has remained ubiquitously in general use, either by itself or together with some of the other GNSS constellations for many different applications, including the ones discussed in this report [6].

How the GNSS-R receiver works:

What follows describes, in broad terms, how one of the most used Navigation receiver designs works.

The Navigation receiver:

The three basic observations: Signal delay (or pseudorange), Doppler shift, and carrier phase are found in the receiver corresponding detection loops: a Delay Lock Loop, a Doppler Delay Loop and a Phase Lock Loop, by comparing them with the delay, Doppler and phase of a receiver-generated model of the signal (synchronized with it when it was transmitted from the satellite using information in the Navigation Message) [1], [2].

The receiver can lock onto the signals, in some newer ones of up to 14 GPS satellites in view from the antenna, and process those of each satellite in parallel, in an equal number of separate signal channels.

The transmitted signals of all GNSS are right-hand circularly polarized (RHCP), with modulated signals for each on carriers out of phase with each other by 90 degrees, known as the:
In Phase (In) and Quadrature Phase (Q) signals.

The Navigation Receiver antenna is fixed to the top of the spacecraft and pointing upwards, oriented so its axis stays aligned to the local vertical. There is a receiver front end for each channel where the antenna signal impedance is matched to the that of front end input, the signals of the different satellites are separated first by frequency and then by their IN Phase, or IP, and Quadrature, or QP, relative polarizations to be processed separately and in parallel, where first each is shifted to a more convenient Intermediate Frequency, then digitized and finally sent to the processing subsystem.

This subsystem consists of two portions: the digital signal detection one, with the various loops for received signal delay, Doppler, and phase, and the Data Processing Module, where signals are sent to be used as data in the Navigation Solution for determining the position, velocity, and phase shift between carrier model and received signal.

All operations following the analog ones in the front-end are made using the digital circuitry of the receiver. This is now more often being implemented as a programmable array of digital gates, or FPGA (Field Programmable Gate Array), where logical gates are connected to hardware elements that are potential interconnection nodes, connected in turn to other such nodes, and where depending on how they are interconnected can implement different receiver architectures. A program is downloaded and read by a separate module that executes it, organizing the delivery of either electrical or light pulses to the various nodes to enable or disable connections between gates and also between nodes, thus forming the intended receiver circuitry in the gate array. Another older kind of programmable receiver still in use is the software-defined receiver, a specialized variant of what is generally known as the "software defined radio." In this type of receiver, the digitized data that are sent from the front end to the receiver digital hardware go instead to a general-purpose computer, for example a laptop, where a program is running that emulates what is done with the hardware of a more conventional receiver. The program can be modified, compiled and run again, as in the case of the type of receiver with FPGA programmable hardware already described. If such a receiver is to be used in a spacecraft, the only part of the computer installed in it is the actual, small-footprint digital hardware, such as the one inside a laptop, plus a small box to contain it, along with the necessary ports, etc.

A third type of receiver is a hybrid one that is software-defined, but some of the calculations are run faster in an attached FPGA module, also programmable. An example of this latter type is the STRATOS receiver [7] carried by the CubeSats of the constellation belonging to the Spire company and that include both the navigation and the reflectometric receiver hardware. This receiver had been used, including its previous version, for doing radio occultations (GNSS-RO) to obtain data on air humidity, temperature, and pressure in the troposphere and the free-electron

content in the ionosphere, along a column of air some hundreds of km deep and a few km wide in front and behind of a satellite so equipped, from close to the Earth's surface to the top of the ionosphere. This receiver is now modified to work also as a GNSS-R receiver. A brief description of this company can be found in the Executive Summary at the beginning of the report, and more is to be found in the section dedicated to it in this body of text.

The advantage of the programable approach is that problems with the receiver can be fixed by troubleshooting and correcting the software that determines the receiver architecture, and future improvements in receiver design can be implemented by simply loading the corresponding program and resetting and reconnecting the digital gates to form this new architecture.

One problem that reduces the quality of the signals received is that of reflections from other objects that are processed together with the useful direct signals. This is known as multipath. It can be a problem on the Earth's surface or close to it in airplanes, where there are objects nearby, or the surface below itself in the case of airplanes. In the case of receivers in satellites, reflections from below are only a problem at very low elevation angles of the incident signals above the antenna plane and even negative ones, as the plane can be small enough for that to happen. This problem is avoided by using only data for satellites above a minimum elevation about the Earth's limb.

The navigation solution requires some preprocessing of the data to eliminate the effect of the ionosphere and tropospheric delays using models for the same, in the case of the ionosphere with the model parameters obtained from the Navigation message, but only useful for surface based and airborne receivers below the ionosphere. So a different approach is used in the case of satellite onboard receivers. As for the phase, the ambiguity consisting in a number of integer cycles of the phase is corrected by one of two kinds of widely used methods: ambiguity resolution or bias estimation.
But, for the most part, the navigation solution is made using the unambiguous code data only. With two different signal frequencies, the ionospheric effect can be eliminated using an ionosphere-free combination of the corresponding two codes.

The receiver clock:

Usually receivers either use a built-in crystal oscillator or are connected to an external frequency standard. The second arrangement is impractical in many applications, so the oscillator is a crystal one. This oscillator produces a signal of more or less constant frequency that is modified with a series of multiplying and dividing phase-lock loops up to the signal carrier and intermediate frequencies. These are modulated with locally generated copies of their signal modulating codes, and the result of this is the receiver signal models that are compared to the incoming ones, to get delay, Doppler and phase shifts in their corresponding detection loops, as already mentioned.

Miniature, chip-scale atomic clocks using as active medium rubidium or cesium vapor, have short term stabilities (1 - 10 seconds) of 10^{-11} - 10^{-12} Their advantage over crystal oscillators (XO) is that they have frequency stabilities comparable to those of oven-controlled ones, used in most precise applications of crystal oscillators, while their power consumption, of the order of

0.1 Watt, is two orders of magnitude less than the oven-controlled crystal ones (OCXO), while their errors vary quite smoothly with time compared with crystal clocks. This greatly simplifies the determination of this type of clock error and its necessary correction. Also, it is easier with such clocks to find and determine the epoch and size of the occasional partial losses of lock known as cycle slips, where the phase suddenly changes by an integer number of cycles, because the cycle slips cannot be not confused with sudden large changes in the clock error, as it could be with crystal oscillators.

The idea of using atomic clock of small size and power consumption low enough to fit well the limited space and power available in a CubeSat is no longer a remote possibility: these days chip-scale atomic clocks, or CSAC clocks are as small as a pack of cigarettes and are also very low- power consumption hardware, their consumption being on the order of one tenth of a Watt. Their short-term stability is orders of magnitude better than an XO and two and comparable to an OCXO. So this is something worth considering for its use in the proposed CubeSat constellation.

https://www.quartzpro.com/ocxofacts.html

https://tf.nist.gov/general/pdf/2178.pdf

2.2) The Reflectometric Receiver:

This receiver is, in some ways, the opposite of the Navigation one described above: the reflections from other objects are a problem with the Navigation one, but are the very signal this one is supposed to receive and process.

The antenna for this receiver points down, towards nadir, while that of the Navigation points up, towards the zenith. Because reflections from water with an incidence angle less than the Brewster angle -- between 52 and 85 degrees for sea water, depending on salt content and density (or, equivalently, a grazing angle between 32 and 5 degrees) [8] -- have their electric field component polarization changed by 180 degrees, the reflected signals are not right hand, but left-hand circularly polarized (LHCP). This means that the antenna should preferably be one that is dual polarized, though right-handed ones have been used in the past, perhaps because there were not many left-handed ones designed to receive the signals at the various frequencies transmitted by GNSS satellites. In principle there is no mystery of how to make such antennas: they should be designed and built as the mirror-images of the right-handed ones.

Also, the way that signals are processed in a reflectometric receiver is quite different. Two potential approaches will be described in some detail, while a third will be described in terms of the general characteristics common to the numerous ways of implementing it. The main difference between the first to be considered and the second (and with many other designs) is that it requires no code demodulation and is only much the same to other types and to navigation receivers in the analog front-end, but quite different in the digital part that follows past the A/D.

The signals received by this receiver and the Navigation one are simply cross-correlated to determine the delay between them. This delay is dominated by the usually brightest reflection,

the one from the specular point, that lies in the plane defined by the position vectors of the GNSS satellite and the LEO. If needed, the instantaneous a priori position of this point can be calculated using the known positions of the GNSS transmitter and the LEO receiver, as well as the known height of the specular point, obtained using a simplified shape, such as an ellipsoid perhaps with some approximated actual shape of the surface (from a Sea Surface Topography map) on it. The solution for obtaining the correction to the calculated 3-D position of the reflection point is only sensitive to first order to the difference in height between the a priori one and the true one. This makes the positioning of the specular point very useful for employing the reflectometer receiver as an altimeter. As the satellite moves along above the Earth's surface, the specular points of the signals of the several GNSS satellites being tracked by the CubeSat receiver move more or less parallel to the CubeSat's ground track at a speed comparable, at some 6 - 7 km/s, to that of the CubeSat carrying the receiver of 7 -8 km/s, each point forming a profile of the true elevation of each surface point minus the calculated one. In the case of the sea surface, a component of this elevation profile may be that of a tsunami, if there is one in the area surveyed. *A key difference between the tsunami component and that of the errors in surface model, etc., used is that the tsunami one changes quickly at every point of the track, as it moves very quickly past it, at 100 - 200 m/s, while the other errors change very slowly, or not at all.*

A second type of receiver tracks the signal reflected from the specular point, using this signal's delay and Doppler shift obtained by adding this point's extra delay and Doppler shift relative to the direct signal, to a copy of the current navigation-receiver model of the signal already aligned in delay and Doppler with the direct signal from the GNSS satellite. The additional shifts in delay and Doppler are calculated with the onboard computer using the known positions and velocities of the GNSS satellite (from the GNSS navigation message) and the LEO (from the receiver's computer navigation solution). Because there are no loops involved in finding this specular point's delay and Doppler, this second type of receiver, slaved as just described to the navigation one, is known as an "open loop receiver."

A third type of receiver consists of the one just described to find the reflections from the specular point and keep track of that point as it moves along the surface, plus a number of similar open-loop receivers, each meant to receive reflected signals with one of a number of different pre-selected pairs of delay and Doppler shift (pairs usually defined in the hardware), as shown schematically in Figure 2. These signals are used to make, with the CubeSat's main computer or with a dedicated co-processor, a Delay Doppler Map (DDM) for each tracked GNSS satellite at every epoch. The DDM and its various uses are described in later sections of this report.

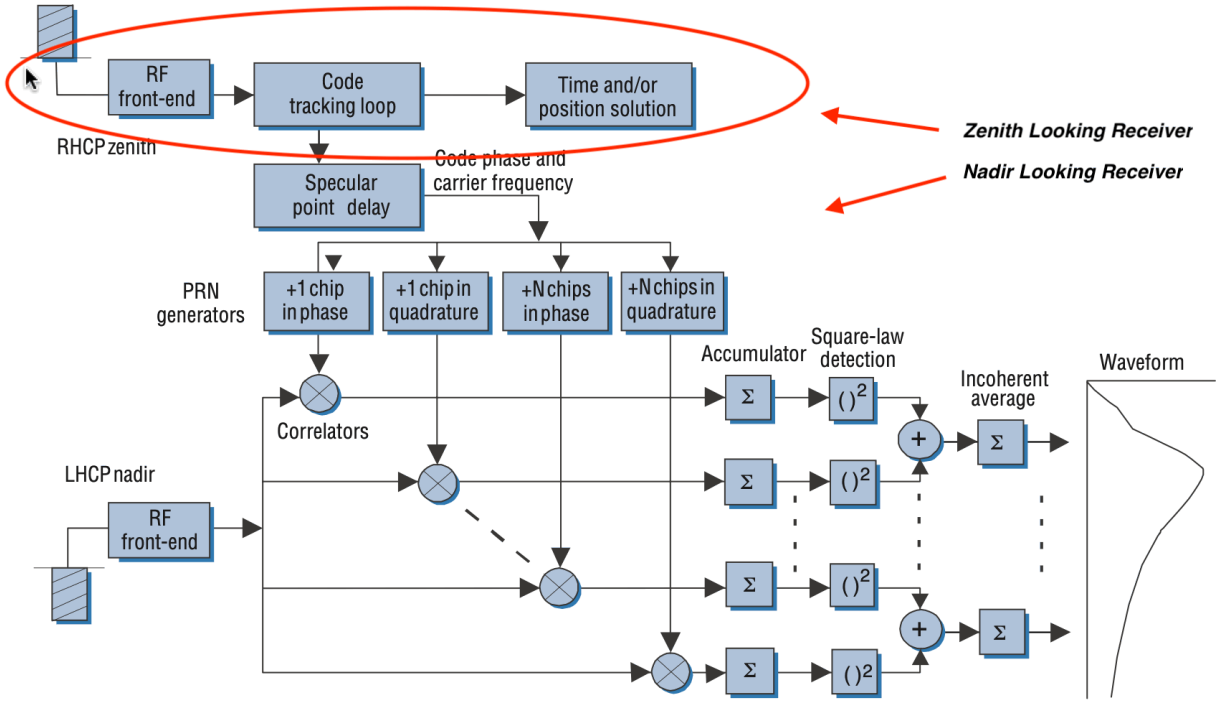

Figure 2. The delay-Doppler-map making GPS receiver acquires reflected signals using a nadir-pointing antenna and direct signals using a zenith-pointing one. The "Waveform" is the plot of delay in the vertical axis vs. (usually) 1-second averaged correlator output for the specular point. This would be the central "zero Doppler" line in the resulting DDM. (From [1] of Section 4.)

This third type of receiver uses a large number of correlators and related components, as shown here. There are other designs that require fewer or none at all. Those receivers are the interferometric ones mentioned earlier in this section. As explained in the "Reflections" section of this report, these points lie on ellipses centered at the specular point and on intersecting hyperbolas where the Doppler shift is constant and different for each one of them. So these intersecting ellipses and hyperbolas define a grid on the Earth's surface, where its nodes are pairs of points with preset delay and Doppler shifts relative to those of the specular point that determines the origin. This information plus the power of the correlated signals can be used to form a three-dimensional map, where the x axis is the Doppler delay, the y axis is the signal's delay and the z axis is the intensity of the correlated signal.

This is known as the Doppler-Delay Map, or DDM, that is very useful and so very much used to study variables related to Global Climate Change, such as wind direction and intensity at sea, especially hurricanes, typhoons, and Southern Atlantic cyclones. The DDM is also useful for studying sea ice extent and condition, snow cover and its depth, soil humidity, lakes and rivers water level, etc. To obtain this map with something other than the receiver hardware architecture just mentioned (which requires as many "receivers" as the number of points in the DDM), there are others that require much fewer and are, therefore, probably of the type of reflectometer receiver to use in CubeSats. In particular, there are other implementations that do not use correlators implemented in hardware but replace them with correlations calculated using the direct and inverse Fast Fourier Transform, carried out in fast and powerful co-processors. The

same computations separate the chosen Doppler-shifted signals required to create, together with the chosen delays, the DDM.

In all cases the analysis of the data is made after the reflected signals are past the front end and already digitized. The processing unit receives information from the Navigation satellite on time and frequency from its clock and other things obtained from reading the Navigation Message that are needed by the reflectometer receiver. The data is corrected before being used, as in the case of the Navigation receiver, for ionospheric and tropospheric delays.

The development of reflectometer receivers is constantly evolving due to the availability of new civilian signals and more suitable electronic hardware, as the technology for making chips that are faster, smaller, less power hungry, and just as reliable as those now in use evolves.

The weaker, diffusely reflected signals have only part of the incident radio waves' power, as this is dispersed in all different directions, and the fact that a significant part of the signal goes into the water. In consequence, the reflectometric data, compared to that from the direct signal captured with the navigation receiver, is much noisier and its phase more prone to partial losses of lock in the receiver known as cycle slips. The latter kind is important, as the effect of these on a solution builds up with time. So the cycle-slips issue has received some serious attention in precise applications that require the use of the carrier phase data, as well as the code delay [7].

References:

[1] Global Positioning System: Theory and Applications, Vol. I, Chapters 3 - 7; the AIAA's series Progress in Aeronautics and Astronautics, Vo. 163, 1996.

[2] Pennsylvania State University Department of Geography explanation of how a GPS receiver detects and uses the signal modulation codes:
https://www.e-education.psu.edu/geog862/node/1756

[3] K. T. Woo, OPTIMUM SEMI-CODELESS CARRIER PHASE TRACKING OF L2, 12th International Technical Meeting of the Institute of Navigation, Nashville, TN, Sept. 14-17, 1999.

[4] Simon, M.K., Lindsey, W.C., "Optimum Performance of Suppressed Carrier Receivers with Costas Loop Tracking," IEEE Transactions on Communications, Vol. COM-25, No.2, Feb. 1977.

[5] International Committee on Global Navigation Satellite Systems, GNSS Receiver Fundamentals.

[6] Masters, D. et al., Status and plans for Spire's growing commercial constellation for GNSS science, International Radio Occultation Working Group Meeting 2022.

[7] Yang Wang; Brian Breitsch; Yu T. Jade Morto: "A State-Based Method to Simultaneously Reduce Cycle Slips and Noise in Coherent GNSS-R Phase Measurements From Open-Loop Tracking" in IEEE Transactions on Geoscience Volume: 59 Issue: 10 - Oct. 2021.

[8] Jin, S.; Cardellach, E.; Xie, F. *GNSS Remote Sensing: Theory, Methods and Applications*; Springer-Verlag: Dordrecht, The Netherlands, 2014.

3) The Reflected Signal, Height Profiles, and the Doppler Delay Map.

GNSS Reflectometry, or GNSS-R uses reflections from land, seas, sea ice, or other icy and snowy regions (cryosphere) to determine various meteorological and geophysical properties that are both of scientific and practical interest: soil humidity, forest canopy biomass, ocean winds, water level in lakes and rivers, sea ice extent, snow depth, etc.

Reflection in real surfaces is a mix of specular and diffusive reflection. Depending on the smoothness or roughness of the reflecting surface, one or the other may dominate.

One characteristic of reflected signals from water surfaces is that part of the signal is not reflected, but goes into the water, and because sea waves have different amplitudes and slopes, the surface is more or less reflective at some places than in others. The combination of this fact and that reflection is diffusive, sending reflected signals in different directions, tends to weaken the reflected signals at the satellite receiver, resulting in poorer signal to noise ratios compared to the reception at the navigation receiver. This results in higher data noise and in more carrier phase cycle slips, caused by losses of signal lock in the GNSS-R receiver data.

The point **Ps** on a reflecting surface, or "mirror", for which the distance emitter-**Ps**-receptor is the shortest, lies at the intersection of the plane of the mirror with a plane perpendicular to it containing both the emitter and receiver of electromagnetic signals and the direct transmission line in between. In the case of a spherical Earth, this point is on a mirror plane tangent to the surface and not far from where it would be on a reference ellipsoidal Earth, or on its actual surface, as long as it is close to the local ellipsoidal horizontal plane. The perpendicular plane to the local mirror in a spherical Earth is the one containing by the receiver, the emitter, and the center of the Earth. Being the point where the distance along the total reflected path between receiver and emitter is the shortest, **Ps**, known as "the **specular point**", tends to be where the reflection is the brightest.

Diffuse reflection, where the surface roughness scatters photons in all directions, is often modelled as Lambertian reflection, proportional in any given reflective direction to the product of the sines of the incident ray and the reflected ray respective grazing angles. This diffusive reflection sends the signal to the receiver by scattering some of it in that direction. Because it depends on the grazing angles, the intensity of the diffuse reflection diminishes quickly away from the specular point **Ps**.

Fresnel ellipsoids and Fresnel zones:

In radio-communications theory, the emitter and receivers are the common focal points of a family of elongated (i.e. prolate) ellipsoids of revolution that contain both points, their common axis being the straight line between transmitter and receiver, or direct transmission line. One important property of these ellipsoids is that if a signal is reflected to the receiver from anywhere in the surface of any one of them, it will reach to the receiver at the same time, a time specific to that particular ellipsoid, traveling the same distance. This common distance being longer than that of the direct transmission, the reflected signals will have a different phase from the one along the direct transmission line. The farther the ellipsoidal surface from the common axis, the

direct transmission line, the greater the phase difference, resulting in the gradually increasing destructive interference between the two. This contributes to the further decrease of intensity of reflections from the specular point.

The ellipsoid where the reflection received from its surface is at 90 degrees from the phase of that from **Ps** is the limit of the First Fresnel Zone, the region where most of the reflected power reaching the receiver comes from. Beyond that, the reflections from a smooth but diffusive surface quickly vanish. Therefore, the intersection of this particular ellipsoid with the reflecting surface is an ellipsoid that contains the brightest part of the reflection. The semi-major axis lies along the intersection of the mirror and the normal plane already defined. The length of this axis depends on the grazing angle at **Ps**, and may range from tens of meters for angles close to 90 degrees, to tens of kilometers for angles closer to five degrees, which can be considered as a practical limit for getting useful reflections.

One can choose the elliptical intersections of successively larger Fresnel ellipsoids as sets of points where all the reflections to the receiver from them, being on the surface of the same Fresnel ellipsoid, must reach the receiver at the same time. Such chosen ellipsoids are therefore equal delay, or isodelay lines.

The delay and Doppler at the specular point shown in Figure 3 become the 0 Delay and 0 Doppler relative to this point, and therefore, the origin of the Delay Doppler Map, or DDM. There is one of these maps per satellite being tracked by the receiver at every epoch. Although they may be created at a lower rate than the one at which the receiver is actually obtaining the data along the specular point tracks, e.g. at 1 per second (or 1 Hz), to be used to obtain vertical profiles of the sea surface along these.

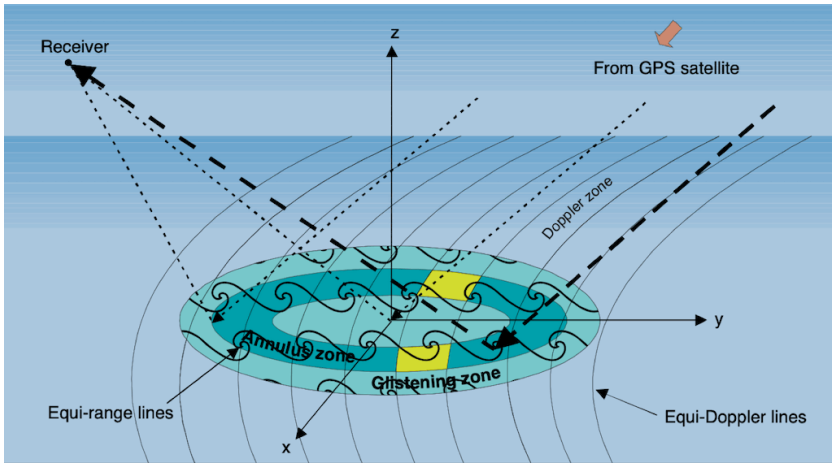

Figure 3. Constant delay (or range, if multiplied by c) ellipses and constant Doppler hyperbolas. These are used also in making a Delay Doppler Map or DDM. Pairs of points such as those in the regions shown here in yellow, with the same delay and Doppler shift cannot be differentiated from each other in DDM maps. The glistening zone is the shinier zone around the specular point where signals are reflected mainly diffusely. (From [1].)

Vertical sea height profiles, from specular-point tracks on the sea surface:

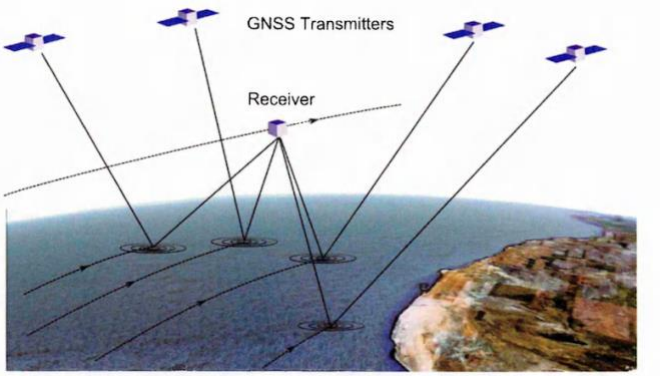

Figure 4. This shows both the first few ellipses of equal delay surrounding each specular point of each GNSS satellite in view from, in our case, a CubeSat. The specular points and ellipses are moving along with the CubeSat at a large fraction of its horizontal velocity in the direction indicated with the arrows in the picture along the tracks they follow on the sea surface.
A LEO satellite in a near circular orbit and an altitude between 550 and 600 km moves with a velocity of some 7 to 8 km/s. (From [2].)

The specular reflection points of the signals from one GNSS satellite move along a line roughly parallel to the LEO satellite subsatellite point, or ground track, and at a comparable speed to that of the LEO satellite. These lines can be translated relatively easily using their reflected data into vertical profiles of the surface height, and would, therefore, reveal a tsunami wave by showing its recognizable height profile, if they happened to run across it. This makes the use of the data from reflections along these lines something of major interest.

The wake effect:

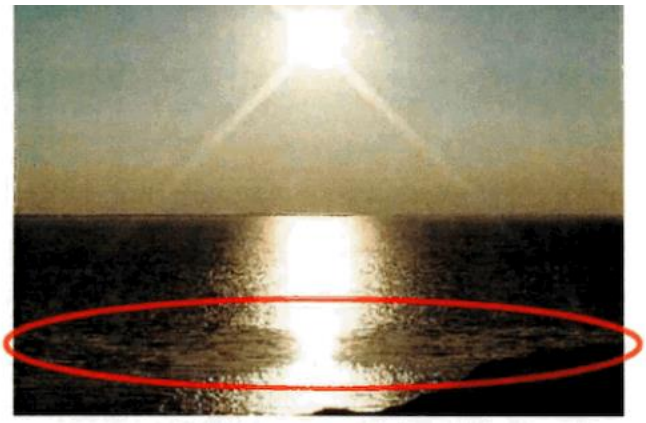

Figure 5. Sunlight is scattered on the sea surface creating a wake. Region of calm water highlighted by ellipse. (From [2].)

A sea wake, as shown in Figure 5, is a long stripe of diffuse reflection centered on the line of maximum intensity, on the plane determined by the position of the transmitter, here the Sun, the specular point and the receiver, a camera lens in this case. The scattering is greater, making the

wake wider, where the water is rougher. This effect also occurs with other electromagnetic waves besides optical ones, for example the radio ones transmitted by GNSS satellites.
This effect makes it possible the use of GNSS-R data to study the effect of surface winds on open waters, particularly stormy ones, from the extent and intensity of the scattered area of the wake.

Doppler, isoDoppler lines and Delay Doppler Maps (DDMs)

There is, however another way in which the reflected signals can be used, and that is to make three-dimensional Delay Doppler Maps, or DDM.
Such maps are made on the basis of the intersections of the chosen isodelay ellipsoids with chosen equal Doppler, or isoDoppler hyperbolas.

What are these?

As the satellite moves along its orbit, the Doppler frequency shift of its signals relative to observers at fixed locations on the Earth's surface is proportional to the projection of the velocity vector along the direction from satellite to observer. The Doppler frequency shift is, therefore, the same along a cone of revolution with its vertex at the satellite and its axis along its velocity vector. The intersections of a family of such cones with the same axis with the reflecting surface form a set of confocal hyperbolas, each for a different Doppler shift, or isoDoppler hyperbolas. All cones have two sides, one pointed forward from the satellite and the other backwards from it, resulting in symmetrical sets of hyperbolas corresponding to positive and negative Doppler shifts, respectively. The hyperbola of zero shift is the axis of mirror symmetry between both sets of hyperbolas. It is a straight line where the vertical plane through the satellite position perpendicular to the one containing both the satellite at any given epoch and the horizontal component of its velocity vector intersects the mirror surface. In the case of GNSS-R, the Doppler measured at the receiver is determined by the instantaneous velocity and direction of movement of both a transmitting GNSS satellite and the receiving CubeSat, resulting in a set of hyperbolas of constant Doppler with similar characteristics to those for a single satellite, as just described, although oriented and positioned differently. (From [4] here and [1] Par. 4.2.1 in Section 4 of this report.)

The zero-Doppler isoDoppler line, on a flat Earth approximation, is a straight line through the subsatellite point, in the case of one satellite, and is also the axis of symmetry of the two sets of hyperbolas for positive and negative Doppler, respectively. In GNSS-R this real zero-Doppler line can be far from the specular point **Ps**, so only the hyperbolas of one of the two sets will pass through the isodelay ellipsoids near this point and appearing to run nearly parallel to each other when plotted just inside the already defined glistening zone near this point and at any possible angle with the ellipsoids' major axes.

The Doppler-Delay Map or DDM:

To make a map of the intersections of hyperbolas and ellipses in a relatively small area centered at **Ps**, the hyperbolas inside this small area will be almost straight lines, and also almost equispaced, when corresponding to equally spaced Doppler shifts. Those away from **Ps** in the

direction of increasing Doppler will have similarly increasingly positive Doppler relative to the one through **Ps,** and those on the other side of the Ps hyperbola will have progressively more negative ones. Subtracting the shift at the hyperbola through **Ps** from each of them, this shifts the Doppler of the **Ps** line to 0 Hz and those of the others to increasingly positive or negative values at, for example, +1 and -1 Hz intervals. These are the modified values of the Doppler coordinate used in the DDM map. The modified values of the delay DDM coordinate are those of the chosen isodelay ellipses minus the delay at the **Ps**, that then has the zero modified delay.

Often this same reasoning, incorrectly employed, is used to justify showing the Doppler lines as symmetrical to the one through the specular point, that is shown as a straight line from where hyperbolas diverge on each side and having their closest approach along the intersection to the vertical plane determined by the transmitter and receiver position vectors with the (reflecting) Earth's surface. The correct general shape of a set of hyperbolas in the proximity of **Ps** is as shown in Figure 3.

Before going on, it must be noted here that the actual curves on a real Earth, not in its flat Earth approximation, are similar to the ones on a flat Earth, somewhat distorted by the surface's curvature and its topography. But when this surface is close to an Earth-fitting oblate ellipsoid and the distance from the specular point is less than 20 km, as it would be the case over a large lake or the sea, this distortion is minor, so it will be ignored in what follows.
Choosing one discrete set of confocal isodelay ellipsoids and one of isoDoppler hyperbolas, these together define a grid made of these intersecting lines on the reflecting surface, as shown in Figure 3, where every intersection point corresponds to one delay and one Doppler shift relative to those at the specular point at its origin.

Using the delay and frequency Doppler shift at each intersection as two coordinates (or as the real and imaginary components of a complex number) and the power of the signal reflected to the receiver there as a third one defines what is known as the 3-D Doppler Delay Map or the 3-D DDM (but usually as just "the DDM"). It moves along with the specular point at its center, as it follows the satellite and at a comparable velocity, forming along the way a continuous series of gradually changing DDM maps of the variably reflecting surface.

Since the same hyperbola intercepts the same ellipsoid at two points, these points have the same delay-Doppler coordinates, creating an essential ambiguity in the grid. There are ideas for resolving this ambiguity using some additional data, but there seems to be no consensus yet about the real usefulness of any of these ideas. Nevertheless, ignoring this ambiguity is not a serious problem when it comes to creating useful DDMs.

The maximum extension of these maps away from the specular point at their origin is chosen as a distance beyond which reflections are unlikely to be strong enough to be useful.

Examples of DDMs:

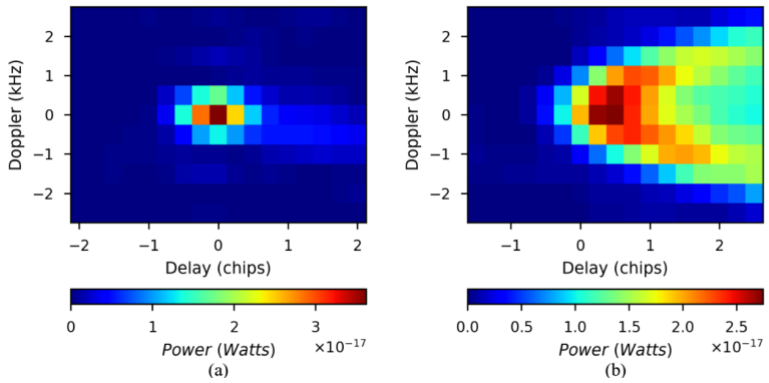

Figure 6. This shows, on the left, a DDM obtained over the relatively smooth bare land of a wheat field in winter and on the right, over rough open waters at sea where waves scatter much more the GNSS signals. Both are typical of such maps over these two types of surfaces. (From [3].)

References:

[1] Komjathy A., Garrison J.L., Zavorotny V., "A New Tool for Ocean Science", GS World, April 1999.

[2] Philip Jales, PhD Thesis "Spaceborne Receiver Design for Scatterometric GNSS Reflectometry", Surrey University, 2012.

[3] Zhounan Dong and Shuanggen Jin, Evaluation of the Land GNSS-Reflected DDM Coherence on Soil Moisture Estimation from CYGNSS Data, Remote Sens. 2021, 13, 570

[4] Dinan Bai, “Modeling of Ocean Surface Delay Doppler Maps Measured in S-Band Signal of Opportunity Reflectometry,” Electrical Eng. Honor Thesis, The Ohio State University, 2022.

4) Tsunami Detection.

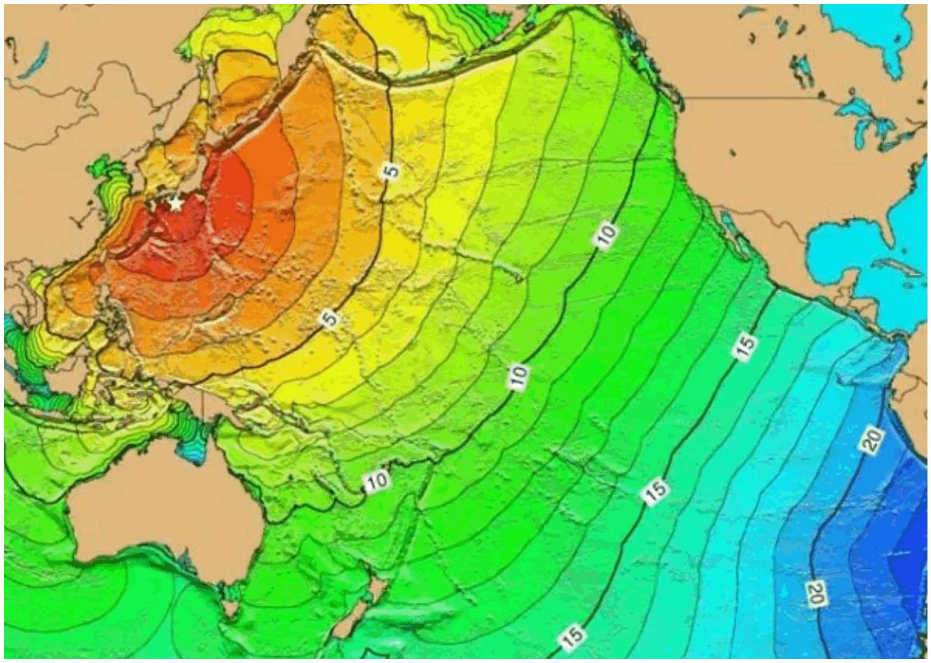

Figure 7. Propagation across the Pacific of the front wave of the tsunami set off by the Tohoku earthquake of 2011 that caused catastrophic damages and loss of life in Northern Japan. Also, it caused inundations and destruction of property in coastal California. (UNESCO International Tsunami Information Center: http://itic.ioc-unesco.org/index.php?option=com_content&view=article&id=1849&Itemid=2563.)

In Figure 7, the numbers in white rectangles are the hours after the start of the tsunami, so it shows it getting to California some 10 - 12 hours later, when it inundated some coastal locations there. Also shown are the locations of submarine mountains and islands, some of which started secondary smaller tsunami (not shown) behind the front wave. The map has been made using a hydrodynamical model of the Pacific Ocean and parts of the Indian Ocean west of Australia.

As the specular reflection points of all the GNSS satellites in view at the various CubeSats overflying the sea follow their corresponding LEO (CubeSat), forming their own tracks on the sea surface roughly parallel to the LEO's ground track, the LEO's reflectometric receiver data can be used to determine the height of the sea above the reference sea surface used as a model, along these tracks as a function of time and at regular measuring intervals (e.g., every second). By calculating the positions of all the specular points at those same epochs using the ephemerides of the GNSS satellites and the LEOs, it is possible to estimate the positions of the specular points, in this way obtaining from every reflection track a vertical profile of the sea surface in latitude, longitude and sea height.

There are several choices of how to do the above and, for example, an idea with a detailed explanation is the one described in [1], Chapter 10, on the detection of tsunami using GNSS-R. There the author describes a method to extract information on the direction, velocity, and

wavelength of the tsunami with data from the several nearly parallel specular point tracks that cross a tsunami's wave in quick succession [2].

Two methods to filter out the data noise are proposed, a noise much larger in the reflected data than in the navigation data and that which is usual when working with GNSS. These two methods are: wavelets and Kalman filtering. After numerous simulations, assuming two levels of Gaussian PDF noise of 10 cm and 20 cm STD, the likely tsunami wave front direction error RMS is, in each case: 4.4 and 5.9 degrees, with a mean of -0.3 and - 0.6 degrees. And in velocity, between 12.7 and 17.7 m/s RMS, with a mean of -0.23 and 0.61m/s respectively.

These estimates should be good enough to predict with sufficient accuracy the position of the wave in the immediate future and can be used to predict the parameters defining the wave based on additional data and the previous profiles. To improve on this requires finding better ways to exploit the unique characteristics of a tsunami: shape, great speed, huge wavelength compared to anything else in the oceans.

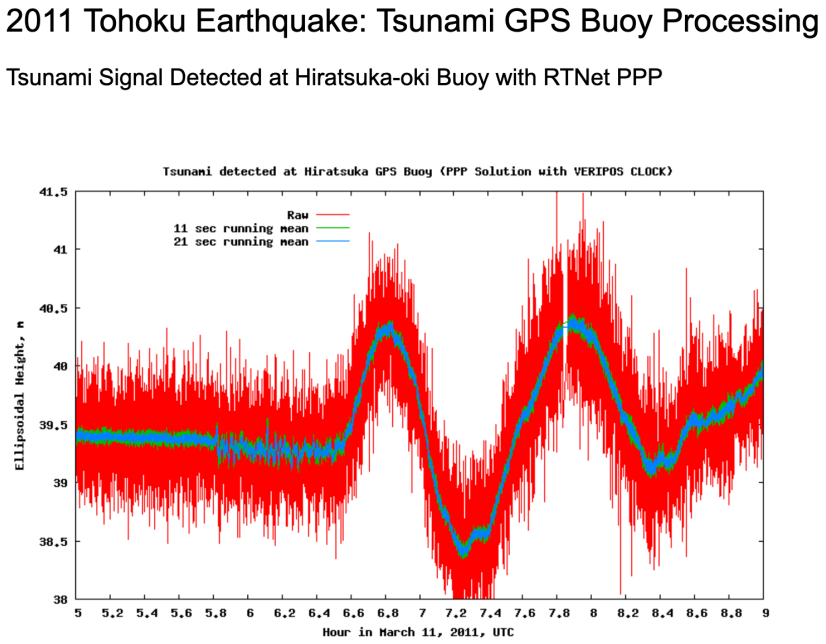

Figure 8. This figure shows the waves of the catastrophic tsunami devastating northern Japan, produced by the very intense Tohoku Earthquake of March 11, 2011. (From [3].)

The waves shown in Figure 8 were recorded at an anchored buoy with a GPS receiver used to make this plot of the buoy vertical movement as the waves went by. The red spikes are very compressed profiles, at this scale, of ordinary waves, of much shorter wavelength (tens of meters vs. hundreds of kilometers). The tsunami is in blue. The vertical profiles along the track of a GNSS satellite specular point would have shown a similar picture, not at a fixed point, but at one moving along this track.

Besides the techniques such as the ones just described for using the reflection tracks of the specular points, an alternative approach shown in Figure 9 is to use the information in the Delay Doppler Map, or DDM [4].

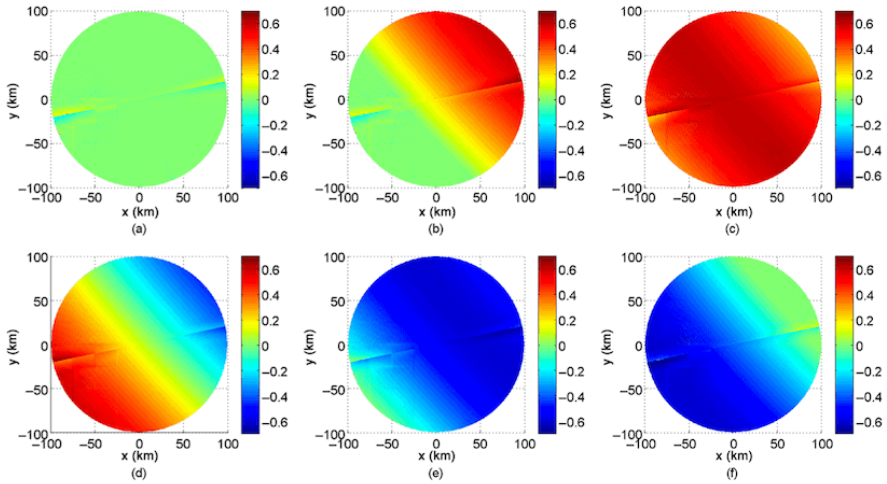

Figure 9. This shows the result of a simulation of successive DDMs of the reflections of a GNSS satellite signals from a passing tsunami wave. (From [4].)

From such a series of plots is clear the direction, speed, and wavelength of the passing wave. While making these kinds of maps is possible, it requires solving a problem first: there are two points with the same delay and Doppler, where a hyperbola in Figure 3 intersects one of the ellipsoids. These two points have, therefore, the same delay and Doppler shift. While there may be one or more ways to resolve this ambiguity, it seems likely that more work is needed.

Except for the still being investigated use of DDM maps, as shown in Figure 9 above, it is necessary to determine even better than with the vertical profile methods mentioned here the main front wave characteristics (direction, velocity, wavelength, size, and position) at epochs sufficiently far into the future to predict reliably the likely time of its arrival at coastal locations. Also important is determining how high above local high tide water mark the arriving waves might reach and how powerful these might be. All this has to be sent as early as possible in messages precise and detailed enough for local authorities to issue on their basis reliable evacuation orders to those at risk of being victims of the resulting devastation when the tsunami reaches their locations.

Complex tsunami wave patterns.

While the vertical profile methods already mentioned are useful for determining mainly the direction and velocity of the front wave of the tsunami, something very valuable for understanding what populations, in which places and when might be in danger, they are not sufficient for making prediction of that over a long period of time, up to 12 hours in the case of one crossing the Pacific from Chile to Japan, for example, travelling across one of its larger dimensions.

Also, as seen in Fig. 10 there is more to a tsunami than its front wave:
Encounters with submarine sea mountains and islands can produce smaller secondary tsunami still powerful enough to need to be tracked. And the reflections on the coastlines, combined with the smaller tsunami, could create an increasingly more complex diffraction pattern across the ocean.
Furthermore, as the speed of the wave depends on the depth of the sea, and this varies, the wave travels at different speeds over places with different depths and as a consequence of all this, it is still a very long wave, but it has no longer a regular, roughly circular shape, as can be seen in Figure 7.

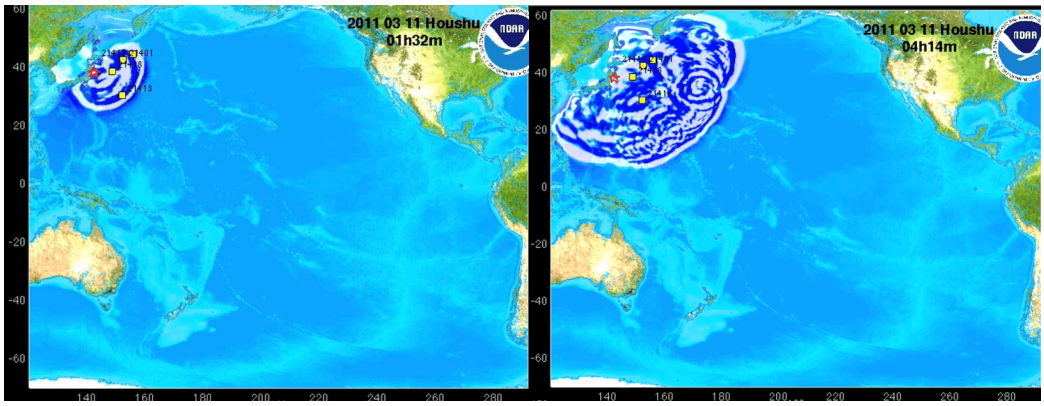

Figure 10. The Tohoku tsunami, as it progressed across the ocean, became more complex behind the front wave, because of smaller tsunami set off by encounters with submarine mountains and islands seen here as sets of circular waves, as well as from coastal reflections and all these secondary waves interferences. (The pictures were grabbed from the NOAA video whose link is immediately below.)

The following URL link is to a NOAA animation of the Tohoku tsunami, showing first the effect of the earthquake and then of the tsunami it caused:

https://www.youtube.com/watch?v=Lo5uH1UJF4A

The tsunami produced by the Tonga volcano explosion:

https://www.youtube.com/watch?v=_fvqWqfrXXM

Combining the reflectometric data with information from other sensors capable of detecting tsunami.

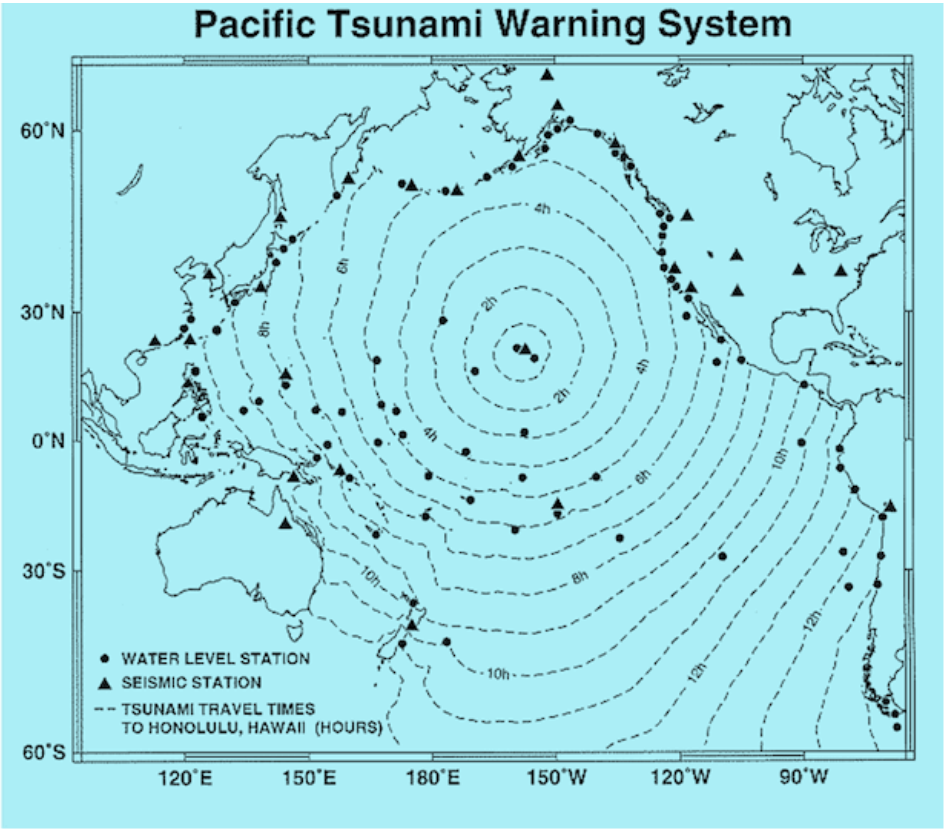

Figure 11. This figure shows the recent geographic locations of the sea-floor pressure gauges of the Pacific Tsunami Warning System. (From [6].)

One way to (a) improve the solution based on GNSS-R and (b) verify the results would be to combine the information from the GNSS-R receivers with that from those of other sensors that are both available and capable of detecting tsunami (for example, the data from pressure gauges deployed at the bottom of the sea to study waves, currents, etc., that can be normally used to learn about the dynamics of the sea). As these tide gauges provide profiles of the waves passing over each of them, they also provide profiles of tsunami, as the waves cross over them and the up and down movement of water changes the pressure at the sea floor accordingly.
The pressure information is sent from the gauges as acoustic signals to buoys above anchored nearby, from where they are transmitted by radio to a place where they are processed to interpret them and issue, if needed, warnings and, or estimates of actual damage to places in danger.
Those operating the CubeSat constellation can likewise use these signals to know when to start real time data processing from the satellite constellation studied here. Clearly, a common effort of a tsunami alert system consisting of several parts is required, of which the constellation would be one important piece.

One Possible Flow Diagram of a Tsunami Warning System

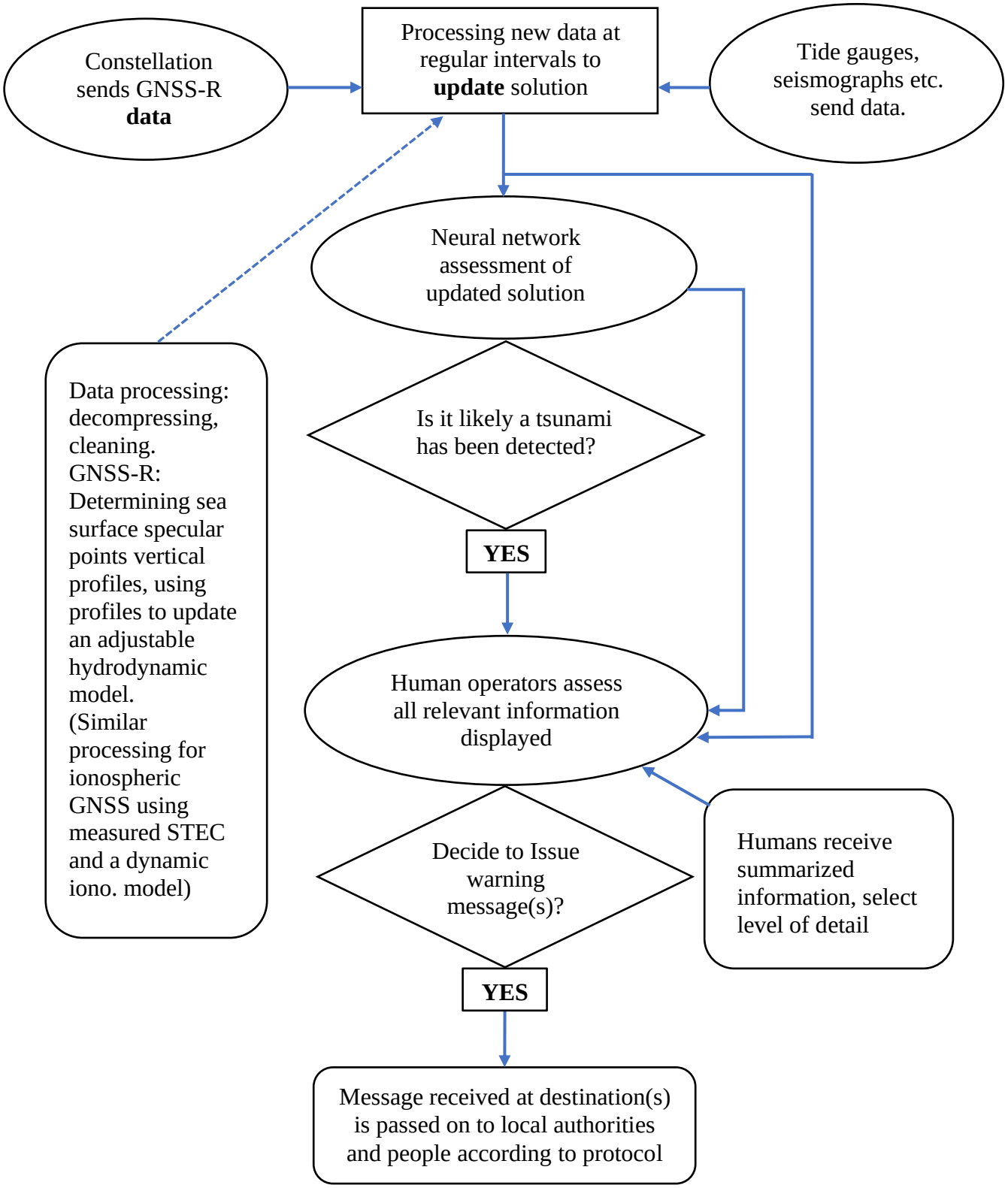

Real-time reflectometry data-driven predictive model.

In what follows, the examples presented are about the reflected signals from the specular point to the reflectometric receiver.

To make progress beyond that, it probably would be necessary to use a hydrodynamic model based on the full 3-D integration of the Navier-Stokes equations. Alternatively, it could be possible to use a linearized, shallow-wave version of them (by this meaning that the tsunami wavelength is much longer than the depth, which is normally the case for tsunami in deep seas), something that is easier and faster to solve, yielding faster results when possible. Such models are run with the bathymetry and coastal outlines as the vertical and horizontal geometric boundary conditions on the solution of the hydrodynamic equations. Usually these models are run off-line, and they get started using the already sufficiently known causes of the movement of the sea floor generating the tsunami: sea cliff collapse, a very large earthquake nearby, etc. This takes time, in particular waiting to have that information available with enough precision may take days. If properly started, such models can be used to find the approximate times of arrival to populated coastal locations, as well as the likely extent and severity, of the resulting inundations, predicted across vast expanses of ocean. For making such predictions timely enough there is no time to wait to get the information on how the tsunami started. Instead, this has to be determined quickly with the data at hand.

One possible approach to doing this in near-real time that should be explored further is the use of the reflectometric data to drive the hydrodynamic model, first for starting it and then for updating it as time goes by. So it remains good enough to still produce and keep improving the predictions, in order to decide if tsunami warnings have to be issued, with what urgency and when.

There has been a number of studies for using this approach to adjust ocean hydrodynamic models assimilating data, for example from tidal gauges, etc., with a recursive Ensemble Kalman filter approach suitable for working with very large state space dynamic systems (see [5] and also [16], [17], [18], [19]) that can be used to model the dynamics of an ocean with a very large number of error states among other things, for example, the velocity vector of the water at the nodes of a 3-D grid. To obtain a reasonably useful a priori tsunami model of the very beginning of it, the initial error states could be fitted to the GNSS-R data at the beginning, using in succession each one of several a priori likely initial states obtained from a gallery of seismic or submarine landslide tsunami triggering events, to find one that best fits the data, and then correcting the filter error states with the same data plus any other relevant data available at the time: from seismographs, tide gages, etc. This then may be repeated at intervals to refine the hydrodynamic model, updating it with the GNSS-R data and other types of data. In fact, the idea here is to combine the CubeSats' GNSS-R data with those from other sensors, when available, making tsunami detection and monitoring an effort involving organizations carrying out monitoring work along some coastal and offshore areas and at scattered deep-ocean locations, for the best possible results.

Because the more urgently needed information is that on the leading wave of the tsunami, the corresponding reflectometric data should be transmitted in real time. Where else the data from

CubeSats passing close by overhead a tsunami should be transmitted as well in real time, is a topic for a further study of this potentially useful approach.

Ionospheric signatures of tsunami, Earthquakes and large explosions, such as volcanic explosions.

The most useful CubeSat GNSS-R data should be that used for obtaining the reflectometric sea height profiles, as well as the observed effect on the ionosphere of gravity and acoustic waves set off by the wave of a passing tsunami as it moves the air immediately above it up and down. These disturbances propagate upwards, eventually into the ionosphere, where they increase in size to a very large extent, as the ionized air density plunges with increasing height. This makes the waves easier to detect in the information obtained by differencing GNSS signals of different carrier frequencies, as the ionospheric delay of the transmitted signals is proportional to the square of their frequencies.

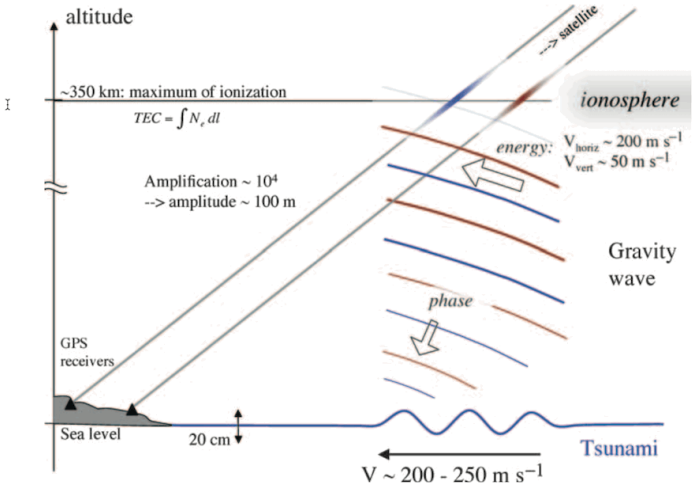

Figure 12. Shown here is the case where the gravity waves are rising through the ionosphere and being detected with GNSS receivers on the ground. But the concept is the same for receivers on CubeSats or any other LEO spacecraft. (From [7].)

By using the free-electron content data obtained from the CubeSats Navigation receivers on the ionosphere above them, together with the one below from the reflectometer receivers data, it may be possible, in principle, to obtain in a short time -- given the dense and continuous world-wide data coverage possible with the proposed constellation -- a map of the whole ionosphere over the oceans and other large bodies of open water or water covered with sea ice, which is an even better reflector than ocean water. Over other types of surface (e.g., land, snow, etc.) the ionosphere above the height of the satellites could still be mapped with the CubeSat's Navigation data.

In places on land there are already many surface GNSS stations that can be and are used to monitor the ionosphere from below. Although their data coverage cannot be compared to that of the CubeSats except with the very dense networks in Japan and California (primarily set up to

monitor seismic activity there), it should be possible to gain more information from the combination of both approaches as well as to calibrate the GNSS-R ionospheric data by comparing it with that from the stations that CubeSats pass nearby.

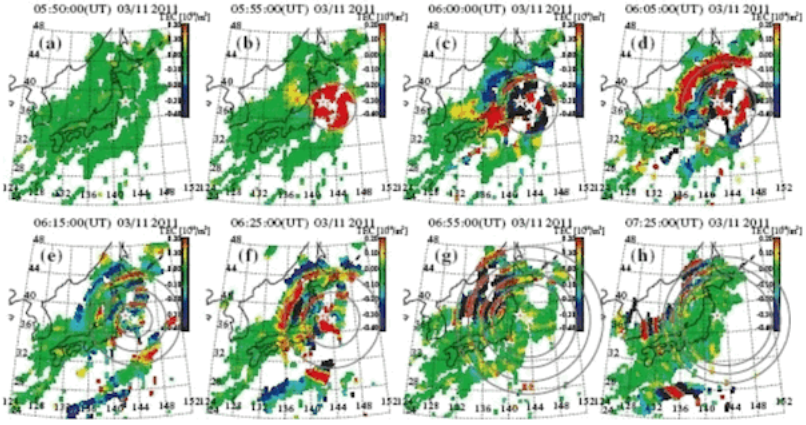

Two-dimensional maps of the detrended TEC from 05:50 UT to 07:25 UT on March 11, 2011. The interval of figures (a–d), (d–f), and (f–h) is 5, 10, 30 minutes, respectively. The star and cross marks represent the epicenter and the ionospheric epicenter, respectively. Gray circles represent concentric circles with the ionospheric epicenter. A movie of the detrended TEC maps with 30-second resolution is available at the NICT website (http://www.seg.nict.go.jp/2011TohokuEarthquake/).

Figure 13. The large tsunami set off by the March 11, 2011 earthquake produced atmospheric waves that reached the ionosphere. Their effect on the data of GNSS stations there, caused by the total free-electron content along the whole paths of the signals from satellites to receivers, can be seen in the plots as numerous small colored circles (mostly green) at the consecutive intervals noted in the original caption. (From [10].)

Japan has the national GEONET network of over 1300 stations equipped with GPS receivers spread across its large Home Islands and on its smaller islands, used primarily to monitor seismic activity. This activity is almost permanent and usually at a low level, but sometimes more intense. This network of stations is run from GEONET's headquarters in the city of Tsukuba [11].

From the point of view of detecting and monitoring tsunami, the mapping of the ionosphere in fine enough detail would reveal also the tsunami-generated waves ascending through it. These consist of gravity waves (so called because they are the result of the interplay of the weight and inertia of the air -- ordinary sea waves are also gravity waves) and acoustic waves. The gravity waves propagate horizontally with the velocity of the tsunami of 100 - 200 m/s but more slowly vertically. It is usually asserted that the vertical speed is of some 50 m/s, but speeds several times greater have been mentioned in the literature. Tsunami may also produce acoustic waves that travel at the speed of sound.

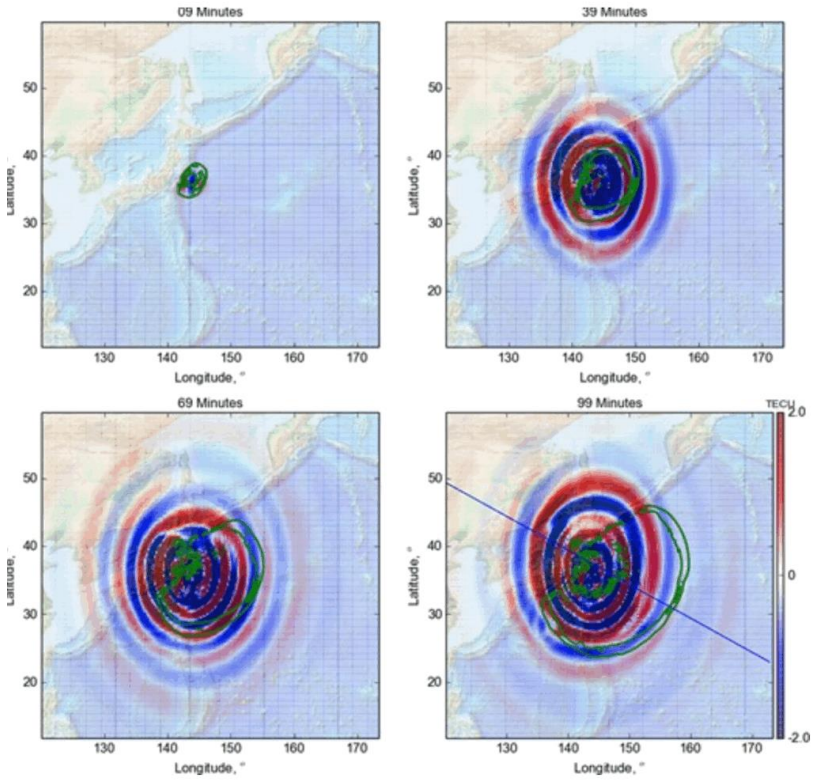

Figure 14. This simulation shows acoustic waves racing ahead of gravity waves as both were being produced by the destructive tsunami caused by the Tohoku earthquake of 2011. (From [8].) The weaker (and paler) acoustic waves propagate faster, ahead of the tsunami ones (green) and the gravity ones (bolder colors) that follow, in turn, the tsunami and acoustic ones. Both acoustic and gravity waves propagate in both vertical and horizontal directions.

Interestingly in this case, the slower gravity waves alone would have arrived to the coasts of Japan almost simultaneously with the tsunami's, where the acoustic ones would have arrived earlier, perhaps being detected soon enough to give a warning that the tsunami, still out at sea, was approaching. It is however unclear in the case of the Tohoku earthquake, where the tsunami started and then arrived in a matter of minutes, if this would have been of much use to those near where the tsunami first arrived. It is likely that there would have been no way to model in time the waves based on the CubeSat data, because the distance to Japan from the submarine earthquake that produced the tsunami, and the one the tsunami had to cross to arrive to shore, was too short and the tsunami too fast to allow enough time for the GNSS-R receiver data to be transmitted, processed, and the results obtained properly evaluated, so an effective warning could be issued. But in other situations, when the earthquake occurs farther out at sea, a useful warning might be issued based on the acoustic waves, not on the slower gravity ones, the results could have been very different for the better.

Finally, from the previous discussion it can be concluded that there are two quite different types of information on a tsunami in progress to be gained from the CubeSats GNSS-R data: one derived from the specular point profiles of sea-surface height, perhaps augmented by the DDM made at the same time, and the other from the imprint of the tsunami on the ionosphere's free-

electron content density, both determined using two different kinds of processing techniques from the Navigation and reflectometric GNSS-R data.

Since the late 1990s, there has been considerable progress made on techniques to map the electron content density in the ionosphere using regular GNSS receiver data [12],[13] that should provide a firm basis for developing those to be used to analyze with the same purpose the proposed constellation GNSS-R data.

Possible use of Physics-based ionospheric 3-D models:

Some ionospheric models (similar to the hydrodynamic models already mentioned) using a physics-based model of the ionosphere [9] make is possible to get a reasonable simulated picture of the real electron content at any given time in three-dimensions. If such a model could be made realistic enough by assimilating all relevant multi-frequency GNSS-R ionospheric data into it, for example using the same Ensemble Kalman Filter approach used with hydrodynamic models, then the ionospheric model might also be driven by the GNSS-R data to show fine enough detail to distinguish these waves from other free-electron density anomalies, for a similar purpose [14], [15], [16].

Other catastrophic natural hazards with ionospheric signatures:

The other natural hazards that can be observed with GNSS data in a manner very similar to the one just outlined for tsunami are earthquakes, volcanic explosions and, also worth mentioning, the impacts of large meteoroids. These require only the information on the ionospheric electron density perturbations caused by the acoustic waves these generate. Otherwise, the concepts just explained also apply to the detection and monitoring of these events, mainly for such things as estimating the extent of the damage that has occurred and to plan for the type and amount of help needed by their victims.

The detection of these events has been studied in recent years using existing constellations of satellites carrying GPS Navigation receivers, whose data are imprinted by the passage of the signals through much of the ionosphere above the satellites, and also using data from other sensors, such as Langmuir probes used to measure in situ the free-electron content along the satellites' orbits [12]. This shall be discussed more fully in the following section.

References:

[1] Kegen Yu: "Theory and Practice of GNSS Reflectometry" in Navigation: Science and Technology series, Vol. 9, Springer Verlag publisher; 2021 1st edition, April 29, 2021.

[2] Yu K, Tsunami lead wave reconstruction using GNSS-R sea surface height measurement. IEEE Transactions on Geoscience and Remote Sensing, 53(5):2603-2611, 2014.

[3] https://www.gps-solutions.com/rtnet_2011_tohoku_earthquake_tsunami

[4] Yan Q, Huang W Tsunami Detection and parameter estimation from GNSS--R delay Doppler Map, IEEE J. Select Topics Applied Earth Observation Remote Sensing, 9(10) 4650 - 4659, 2016.

[5] Evensen, G. (2003). "The Ensemble Kalman Filter: Theoretical Formulation and Practical Implementation". Ocean Dynamics. **53** (4): 343–367.

[6] http://www2.tulane.edu/~sanelson/Natural_Disasters/tsunami.htm

[7] Juliette Artru, Vesna Ducic, Hiroo Kanamori, Philippe Lognonne´ and Makoto Murakami, Ionospheric detection of gravity waves induced by tsunamis, Geophys. J. Int. (2005) 160, 840–848

[8] E.A. Kherani, L. Rolland, P. Lognonne´, A. Sladen, V. Klausner and E.R. de Paula, Traveling ionospheric disturbances propagating ahead of the Tohoku-Oki tsunami: a case study, Geophys. J. Int. (2016) 204, 1148–1158.

[9] X. Meng ,O. P. Verkhoglyadova,A. Komjathy,G. Savastano,A. J. Mannucci, Physics-Based Modeling of Earthquake-Induced Ionospheric Disturbances,
Journal of Geophysical Research: Space Physics / Volume 123, Issue 9 / p. 8021-8038 Research, 2018.

[10] Tsugawa, T., Saito, A., Otsuka, Y. et al. Ionospheric disturbances detected by GPS total electron content observation after the 2011 off the Pacific coast of Tohoku Earthquake. Earth Planet Sp 63, 66 (2011).

[11] https://www.gsi.go.jp/ENGLISH/geonet_english.html

[12] Hernández-Pajares, M.; Juan, J.M.; Sanz, J.; Colombo, O.L. Application of ionospheric tomography to real-time GPS carrier-phase ambiguities resolution, at scales of 400–1000 km and with high geomagnetic activity. Geophys. Res. Lett. 2000, 27, 2009–2012

[13] Lul W. , Guanyi Ma G., and Wan Q., A Review of Voxel-Based Computerized Ionospheric Tomography with GNSS Ground Receivers, Remote Sense, 2021, 13(17), 3432.

[14] Morozov, A. V., Ridley, A. J., Bernstein, D. S., Collins, N., Hoar, T. J., & Anderson, J. L. (2013). Data assimilation and driver estimation for the global ionosphere-thermosphere model using the ensemble adjustment Kalman Filter. J. of Atmos. and Solar-Terrest. Physics, 104, 126–136.

[15] S. M. Codrescu ", M. V. Codrescu, M. Fedrizzi, An Ensemble Kalman Filter for the Thermosphere-Ionosphere, Space Weather, Vol. 16, 1, 57-68, 2018.

[16] Ridley A., Deng Y., Tóth G., The Global Ionosphere-Thermosphere Model, Journal of Atmospheric and Solar-Terrestrial Physics, 2006.

[17] Evensen, G.: Sequential data assimilation with a nonlinear quasi-geostrophic model using Monte Carlo methods to forecast error statistics, J. Geophys. Res., 99, 10143–10162, 1994.

[18] Penny, S. G., Kalnay, E., Carton, J. A., Hunt, B. R., Ide, K., Miyoshi, T. and Chepurin, G. A.: The Local Ensemble Transform Kalman filter and the running-in-place algorithm applied to a global ocean general circulation model, Nonlinear Process. Geophys., 20(6), 1031–1046, doi:10.5194/npg-20-1031-2013, 2013.

[19] Ohishi S., Hihara T., Aiki H., Ishizaka J., Miyazawa Y., Kachi M., Miyoshi T., An ensemble Kalman filter system with the Stony Brook Parallel Ocean Model v1.0, Geosci. Model Dev., 15, 8395–8410, https://doi.org/10.5194/gmd-15-8395-2022, 2022.

5) Detection of Large Earthquake and Volcanic Activity.

Large earthquake detection:

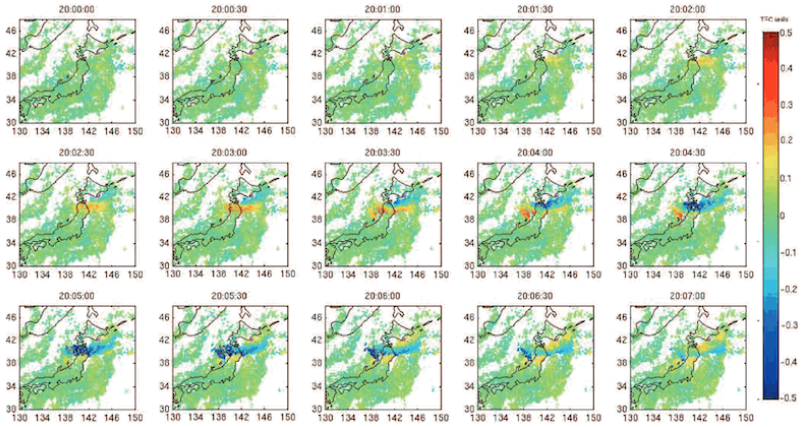

Figure 15. The effect on the ionosphere above and around Japan of the Tohoku earthquake as captured and mapped with data from the very dense GEONET network of GPS stations. A spectacular ionospheric perturbation is observed near the source, corresponding mostly to acoustic waves generated by the Earthquake (From [1].)

The GEONET network of GPS stations is operated in Japan primarily for monitoring seismic activity, as this causes the stations to move and change positions, a movement that can be detected almost instantly by processing in real time, at the Tsukuba headquarters, the data from its over 1300 receivers distributed nation-wide. Here the data was used offline, as in the case of Fig. 13, to later map the ionospheric fluctuations, as shown above. The earthquake seismic waves travelling through land from the north to the south of Honshu island generated mainly acoustic waves that followed the vertical motion seismic Rayleigh waves along the island.

As explained in [1]: "The seismic waves with the largest ground amplitude are the surface waves and especially the Rayleigh waves. They propagate along the Earth's surface, in the crust or upper mantle, with velocities ranging from 3 to 4 km/s. For large and superficial quakes, their displacement amplitude, even at an epicentral distance of 10000km, can reach several mm or even cm, as was observed after the large Sumatra earthquake of December, 26, 2004. The propagation speed of the wave front being much larger than the sound speed in the atmosphere, the generated air waves propagate almost vertically from the surface location of the Rayleigh wave front. With their long periods (T > 10-20 s), the infrasonic atmospheric waves are not attenuated by the atmospheric viscosity: they propagate with a constant kinetic energy and therefore, their amplitude grows exponentially as the inverse of the square root of density. As shown by Fig. 1, the density decays by 10 orders of magnitude between the ground and 200 km of altitude and amplification of 10^5 can therefore be encountered by air waves during their upward propagation."

Large volcanic activity detection:

The Tonga Hunga Ha'apai underwater volcanic explosion of 15 January 2022 was the most powerful ever recorded, sending a huge plume of ash, gases, and water to a height of 50 - 55 km into the mesosphere in such quantities that it cooled detectably the whole atmosphere and producing also such a violent overpressure blast wave that it circled the world several times and was measured with barometers in meteorological observatories around the world. The initial powerful wave was a Lamb pressure wave and it was followed by others of this low-atmosphere waves. These waves expanded circularly from the explosion at close to the speed of sound: the pictures in Fig. 16 below show an area the includes Japan and part of Australia [2]. They also set off a powerful tsunami that reached to distant shores.

Contrasted with the special case of the Japan tsunami and earthquake shown in previous examples, based on that country's GPS observations made with GEONET (the very dense nation-wide network of stations being continuously operated there to monitor seismic movements), the much fewer ionospheric signatures, indicated with colored spots in the figure, shows the sparsity across the world and particularly across the oceans (where it is limited to a few larger islands) of stations continuously operating in support of geodesy and other sciences with generally available data.

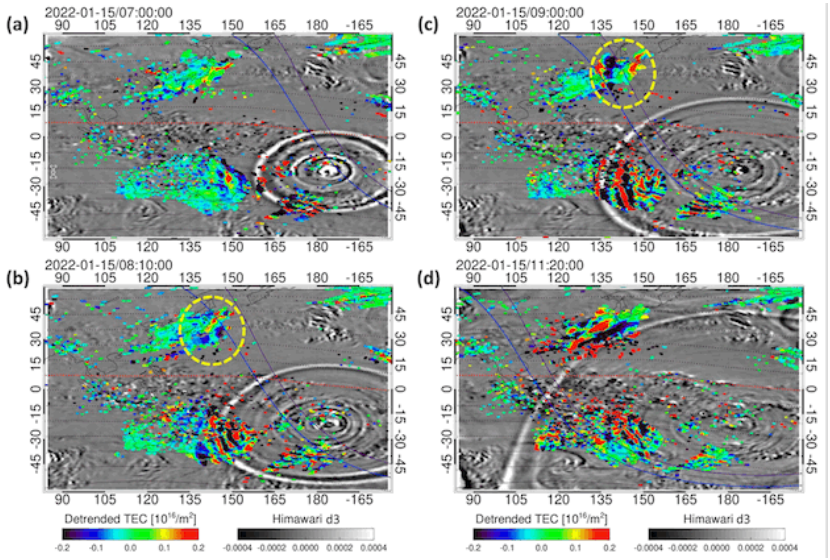

Figure 16. Plot of the waves generated by the explosion made using several different types of data, including the Total Electron Content (TEC) from regional GNSS ground stations, measured along the path of the radio waves from satellites to receivers in Japan and Australia, shown in color, and the lower atmosphere pressure Lamb waves, in grey. The effect of the passing ionospheric waves over Japan is shown within a dashed yellow circle (From [2].)

Quoting from the abstract of Reference [2]: " ... we analyze Global Navigation Satellite System-total electron content data and ionospheric plasma velocity data obtained from the Super Dual Auroral Radar Network Hokkaido pair of radars. Further, we use thermal infrared grid data with high spatial resolution observed by the Hima- wari 8 satellite to identify lower atmospheric

disturbances associated with surface air pressure waves propagating as a Lamb mode. After 07:30 UT on 15 January, two distinct traveling ionospheric disturbances propagating in the westward direction appeared in the Japanese sector with the same structure as those at magnetically conjugate points in the Southern Hemisphere."

This online article includes a video of the blast wave expanding along the part of the Earth's globe visible from the NOAA GOES-West Geostationary Weather satellite on the infrared clouds observing channel:
https://eos.org/articles/the-surprising-reach-of-tongas-giant-atmospheric-waves

References:

[1] Philippe Lognonné 1, Raphael Garcia 1, François Crespon 1, Giovanni Occhipinti 1, Alam Kherani 1 and Juliette Artru-Lambin 2, Seismic waves in the ionosphere, europhysics news, number 4, volume 37, 11.

[2] Shinbori et al., Electromagnetic conjugacy of ionospheric disturbances after the 2022 Hunga Tonga-Hunga Ha'apai volcanic eruption as seen in GNSS-TEC and SuperDARN Hokkaido pair of radars observations, Earth, Planets and Space (2022) 74:106

6) GNSS-R as a Tool for Monitoring Global Climate Change.

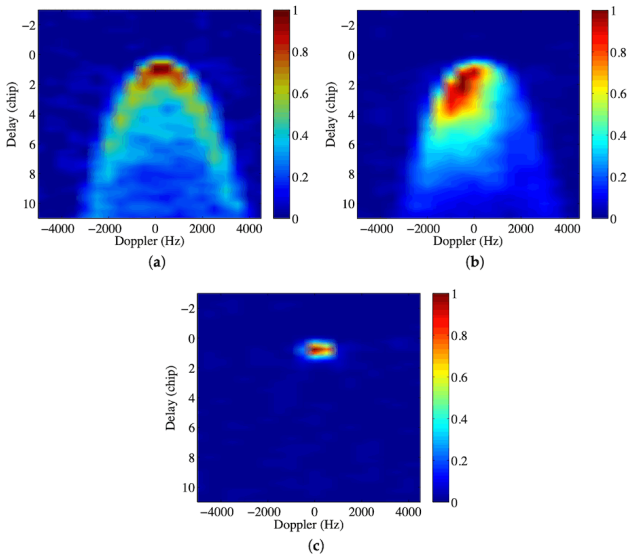

Figure 17. Three DDMs, one showing the diffuse reflection from (a) wind-driven waves in rough open sea water; (b) mix of open sea water and ice; (c) 100% smooth sea ice. (Reference [1]).

Figure 17 shows how different aspects of the sea surface under possibly strong winds, with different levels of sea ice on it, can be seen and studied with DDMs. This is one example of how DDMs are used for monitoring diverse properties of the Earth's surface related to Global Climate Change. In this case, surface wind on open waters and with various degrees of sea ice coverage. Notice that sea ice is generally smoother and therefore much more specularly reflective than the sea surface with its often-large wind-driven waves, as the ice surface irregularities are often smaller than the GNSS reflected signals' wavelength.

While the main purpose of the proposed CubeSat mission is to detect, track and determine the danger posed to coastal communities by tsunami, the same data can be collected not just over the oceans and transmitted in real-time to a center for later processing. Because the GNSS-R data, received offline from regular data dumps to ground stations and archived for later processing, collected in this way when there is no tsunami in progress, or there isn't the occurrence of the other natural hazards that is vital to observe in real time, but are infrequent events, the same data can be utilized off-line to monitor important processes that are relevant to monitoring Global Climate Change.

The study of aspects of climate change observed using the direct and reflected signals of GNSS satellites received in CubeSats carrying GNSS-R receivers has been under way for years now and still goes on, becoming ever more active, while the techniques for extracting such information obtained with those receivers continue to develop and become more sensitive to climate change indicators.

Among others, these indicators are measures of:

- Sea level rise, with the CubeSat constellation densifying, with their oceans-wide and very closely spaced, if noisy, observations of sea heights, the very precise altimetry data (but with sparser coverage) obtained with satellite altimeters in missions such as NASA's Jason-3, or ESA's Sentinel-3.
- Water level in lakes, lagoons, rivers.
- Storms and corresponding precipitation and wind strength.
- Extent of coverage and properties of ice in polar regions and high mountainous areas.
- Extent and depth of snow cover, including those polar regions.
- Humidity of the soil, for monitoring the capability of growing staple crops in areas affected by severe draughts and advancing desertification.
- Wetland conditions.
- Biomass of prairies and forests.
- Effect of global warming on the ionosphere, such as its cooling, as greenhouse gasses trap below it some of the surface radiated heat that would otherwise make it warmer.

Below, a few examples of publications online, with quotes taken from their abstracts, are about satellite missions using GNSS-R techniques for obtaining information on some of the above mentioned and also on other indicators of climate change:

HydroGNSS (Hydrology using Global Navigation Systems' signals)

https://ieeexplore.ieee.org/stamp/stamp.jsp?arnumber=9456091

Martin et al., *An Introduction to the HydroGNSS GNSS Reflectometry Remote Sensing Mission*, IEEE Journal of Selected Topics in Applied Earth Observations and Remote Sensing, Vol. 14, 2021 6987, doi: 10.1109/JSTARS.2021.3089550

Quote: "Satellite System reflections have been selected as the second European Space Agency (ESA) Scout earth observation mission to demonstrate the capability of small satellites to deliver science.
This article summarizes the case for HydroGNSS as developed during its system consolidation study. HydroGNSS is a high-value dual small satellite mission, which will prove new concepts and offer timely climate observations that supplement and complement the existing observations and are high in ESAs earth observation scientific priorities.

The mission delivers the observations of four hydrological essential climate variables as defined by the global climate observing system using the new technique of GNSS reflectometry. These will cover the world's land mass to 25 km resolution, with a 15-day revisit. The variables are soil moisture, inundation or wetlands, freeze/thaw state, and above-ground biomass."

Global Navigation Satellite System Reflectometry (GNSS-R) algorithms for wetland observations

https://ieeexplore.ieee.org/document/8127155

Zuffada, C., Chew, C., and Nghiem, S. V., *Global Navigation Satellite System Reflectometry (GNSS-R) algorithms for wetland observations*, 2017 IEEE International Geoscience and Remote Sensing Symposium (IGARSS), 2017, pp. 1126-1129, doi: 10.1109/IGARSS.2017.8127155

"It is important to closely monitor the state of the world's wetlands, as climate change and human encroachment in a rapid global urbanization trend threaten to cause large-scale wetland collapse. Because wetlands are often difficult to observe in situ, remote sensing is the only viable way to map wetland extent globally. However, current remote sensing methods suffer limitations in capturing wetland extent, and more importantly, wetland dynamics at appropriate spatial and temporal scales. GNSS-Reflectometry could help fill the current observation gap, as experimental data show that ground-reflected GNSS signals are very sensitive to changes in inundated areas. Furthermore, because this technique only requires a custom developed receiver and antenna system, a constellation of such instruments can potentially be launched at relatively low cost, providing global observations at sub-daily intervals. One challenge remains, however, which is quantitatively formulating the geophysical product of reflections over the land surface in various states of inundation. Here, we use a novel reflection dataset, derived from the SMAP radar receiver, to elucidate the sensitivity of reflections to small land surface features and their seasonal variations. Additionally, we quantify the dynamic range of reflections over both open and closed wetlands, and suggest an algorithm for wetland type classification."

Polarimetric GNSS-R Sea Level Monitoring Using I/Q Interference Patterns at Different Antenna Configurations and Carrier Frequencies

https://ieeexplore.ieee.org/document/9585474

Rajabi et al., *Polarimetric GNSS-R Sea Level Monitoring Using I/Q Interference Patterns at Different Antenna Configurations and Carrier Frequencies*, IEEE Transactions on Geoscience and Remote Sensing, vol. 60, pp. 1-13, 2022, Art no. 5801613, doi: 10.1109/TGRS.2021.3123146.

"Coastal sea level variation as an indicator of climate change is extremely important due to its large socioeconomic and environmental impacts. The ground-based global navigation satellite system (GNSS)-reflectometry (GNSS-R) is becoming a reliable alternative for sea surface altimetry. We investigate the impact of antenna polarization and orientation on GNSS-R altimetric performance at different carrier frequencies. A one-year dataset of ground-based observations at the Onsala Space Observatory using a dedicated reflectometry receiver is used.

Interferometric patterns produced by the superposition of direct and reflected signals are analyzed using the least-squares harmonic estimation (LS-HE) method to retrieve sea surface height. The results suggest that the observations from global positioning system (GPS) L1 and L2 frequencies provide similar levels of accuracy. However, the overall performance of the height products from the GPS L1 shows slightly better performance due to more observations. The combination of L1 and L2 observations (L12) improves the accuracy up to 25% and 40% compared to the L1 and L2 heights. The impacts of antenna orientation and polarization are also evaluated. A sea-looking left-handed circular polarization (LHCP) antenna shows the best performance compared to both zenith- and sea-looking right-handed circular polarization (RHCP) antennas. The results are presented using different averaging windows ranging from 15 min to 6 h. Based on a 6-h window, the yearly root mean squared errors (RMSEs) between GNSS-R L12 sea surface heights with collocated tide gauge observations are 2.4, 3.1, and 4.1 cm with the correlation of 0.990, 0.982, and 0.969 for LHCP sea-looking, RHCP sea-looking, and RHCP up-looking antennas, respectively."

Implementing GNSS-Reflectometry in Space on the TechDemoSat-1 Mission

https://www.ion.org/publications/abstract.cfm?articleID=12373

Unwin, M., Duncan, S., Jales, P., Blunt, P., Tye, J., "Implementing GNSS-Reflectometry in Space on the TechDemoSat-1 Mission," *Proceedings of the 27th International Technical Meeting of the Satellite Division of The Institute of Navigation (ION GNSS+ 2014)*, Tampa, Florida, September 2014, pp. 1222-1235.

"TechDemoSat-1 (TDS-1) is SSTL's latest technology demonstration mission, hosting cutting-edge UK payloads including the SGR-ReSI, the company's most advanced Global Navigation Satellite System (GNSS) Reflectometry (GNSS-R) remote sensing instrument. GNSS-R is the measurement of GNSS signals reflected off the Earth's surface. These signals should contain the geophysical imprint of the Earth's surface, be it the ocean, land or ice. The primary target of SSTL and its partner, the National Oceanographic Centre (NOC), is the use of GNSS-R to determine ocean roughness, wind speed and wind direction. Potential applications for ocean surface GNSS-R include weather forecasting, climate change modelling, and logistical planning in the offshore energy and shipping industries. This paper gives an overview of the reflectometry algorithms used on the SGR-ReSI, the interfacing and the methods of testing, and the configuration of the experiment on TDS-1. TDS-1 was successfully launched on a Soyuz-2 launcher on 8th July 2014. This paper describes the early operations and results from the SGR-ReSI on TDS-1, showing the successful acquisition of both raw data and Delay Doppler Maps over Atlantic and Pacific Oceans. A campaign is being planned with support from ESA to allow the cross-correlation with buoys over a wide range of sea state conditions, with the intention of demonstrating an ocean wind measurement service. The SGR-ReSI has minimal impact upon spacecraft system design, being compact, low power and with a low data rate output. It is therefore ideally suited for use on flights of opportunity as they arise in SSTL's own missions and for constellations of small, low-cost spacecraft. The SGR-ReSI will be flying as the primary payload on CYGNSS hurricane-sensing constellation, funded under NASA's Earth Venture 2 programme."

7) Data Transmission.

Real-time communication CubeSat-to-ground and vice versa.

Two-way telephone communication via LEO comsats:

The number of data bits per second corresponding to the acquired data may be fairly large, depending on what is being sent.
In the case of the download of the data considered here from a CubeSat via a communications link, this number could be quite considerable.

In such a case, one possible solution would be to transmit the most voluminous data type (e.g. the DDM one) at a sufficiently low rate that there is enough time to transmit all of such data for one single epoch every N seconds, spreading its transmission over those seconds, in this way dividing the necessary bandwidth by N. As well as compressing the data to reduce the volume to be transmitted, in some way that can be decompressed on the ground processing site without any loss of information in the process.

Here follows a discussion on the possibility of using the satellite telephony provided with low earth orbit satellite transponders by commercial satellite communication services (satcoms), such as the Iridium constellation.

The Iridium Constellation services and available channel bandwidths:

The following has been excerpted from this online article:

https://m-cramer-satellitenservices.de/en/basics-solutions/iridium-satellite-network/

"*Iridium, this is a global satellite communications system consisting of a total of 66 active and 6 reserve satellites, for a total of 72 satellites. Originally, 77 satellites were planned; 77 is the atomic number for the chemical element iridium.*

With Iridium NEXT, a new satellite network has been installed since December 2018, which allows data rates in the Iridium Certus service of up to 700 kbps, making internet and other digital services possible for special data terminals. Up to 1.4 Mbps is planned in a further expansion stage. Iridium Certus is available for use on land and at sea (maritime).

Iridium has been approved for the Global Maritime Distress and Safety System (GMDSS) as part of the innovations.

The main advantage of a satellite-based communications system is that large areas can be covered without terrestrial stations. The terminals communicate directly with the satellites. The satellite network is connected to the existing terrestrial telephone and internet network via several gateways (ground stations). Iridium devices can be used absolutely globally.

In the case of Iridium, the individual satellites are additionally connected to each other by inter-satellite links (ISLs). An active connection is mediated from satellite to satellite until one of these is within range of a gateway. The connection then finds its way into the terrestrial networks via this ground stations.

This makes possible for satellites in low earth orbits to continuously maintain communications with the ground, receiving and transmitting data on demand and in real-time. Satellites in lower orbits typically include those used for climate observations and disaster relief efforts, as well as a host of other applications. Traditionally, these satellites have had to wait until they came back into range of a ground station before being able to receive tasking information and transmit telemetry and valuable collected data. The new data link should reduce waiting times for such data transfers from several hours to a handful of minutes. This can enhance life-saving efforts in a natural disaster or enable observers to spot issues and direct resources to tackle them before they develop or get out of hand.

The transmission power of cell phones is limited for health reasons. To enable a connection to be established, the satellites must therefore be in a low earth orbit. The Iridium satellites orbit the earth at an altitude of about 780 km in six nearly polar orbits (orbital inclination = 86.4°), each with eleven functioning satellites and one reserve satellite per orbit. A satellite needs about 100 minutes to orbit the earth, and about 10 minutes from horizon to horizon. Due to the polar orbits, the coverage density at the poles is particularly high. Until today, Iridium is the only satellite network that guarantees coverage at both polar caps."

Furthermore, NASA has already dealt with Iridium in connection to at least one earlier small satellites mission [1].

One idea for further consideration is whether the use of intersatellite radio links, such as those of the Iridium satellites (and GNSS ones) might provide advantages worth adding such equipment with the consequent increase in the power requirements and the weight of each CubeSat.

In what follows, a form of lossless compression that can be applied to data to reduce greatly the number of bits that have to transmitted, shall be considered.
In this section are not considered error detection code's extra bits, or those used as flags to mark various issues, nor time stamps or other components of a data message, as the data transmitted is, by far, the one item to use up the most bits in a transmission, unless effectively compressed.

The use of the **Iridium** example is intended here only to show what would be needed to use such a service for real-time communication between a CubeSat and a ground processing facility. What might be available at the time when an actual mission is implemented could be different, but considering the present trends in Internet and telephony-relaying constellations of satellites, there is likely to be by then available an even more convenient choice of satellite telephony systems.

The Iridium company, at the moment, provide their "Certus" users telephony service plans at standard rates ranging from 20 MB/minute through 10,000 MB/minute. The corresponding

prices recently ranged from $0.60 through $0.95, depending on the MB/minute rate and whether the service was intended for Maritime or Land use.
Further, it also offers transmission rates for special applications, including for Internet connection, of 22 - 704 Kb/s. This probably should be enough for the transmission of the CubeSat data considered here and even more.

Upon examination of the size of the telephone equipment needed on board each satellite, the corresponding antenna size and the overall power consumption, these seem to be small enough for use in a CubeSat. Furthermore, transmission could be better and the power consumption needed to transmit the data, less than from the ground, as every CubeSat proposed orbit is at a height of 230 km or less than that of the Iridium ones that orbit at some 780 km, so they are more than three times closer than using the same terminals from the Earth's surface.

Now let us consider the transmission bandwidth needed to send first (a) the navigation receiver data and then (b) the quite noisy GNSS-R data imperfectly reflected from the surface below. The relevance of the number of bits used here shall be justified further on in this section.

Approximate number of bits to be transmitted for uncompressed: code (delay) and phase, each corresponding to over 20,000,000 meters straight-line distance between the CubeSat receiver antenna and the GNSS satellite transmitting antenna, assuming a resolution of 1 mm, require (roughly speaking) 35 bits per GNSS satellite tracked, code or phase only, 1 frequency, or 70 bits for both phase and code, or 140 bits for 2 frequencies. Or 140x10x [No. of GNSS] for 10 satellites tracked simultaneously of each of three GNSS systems. In the case of high-rate, one observation per second, as during the overfly of a tsunami front wave, this would come to 4200 bits/s (or Bauds: 1 Baud = 1 bit/s). Or, equivalently per minute: 4200 x 60 = 252,000 bits per minute = 31,500 MB/minute. This clearly exceeds by more than a factor of three the capacity of the regular subscribers' "Certus" service with the largest bandwidth.

However, the highest bandwidth on offer at present for special applications is that of the "Certus 700", service with 704 Kb/s, which greatly exceeds the mentioned 4.2 Kb/s bandwidth.
So, depending on present needs, one could use the current subscriber service with the highest data cap per minute, or sample the data at 3 or 4-second intervals, to fit this system available capacity, or compress the data at least as many times using some lossless method.
Or use a higher Kb/s service, such as the Certus 700, that operates in the L-Band. This apparently does not interfere with the GNSS receivers onboard terrestrial vehicles (airplanes, ships, etc.) Whether it might do so at the proposed CubeSat constellation altitude is an open question.

Nevertheless, it is useful to explore further possibilities, to consider ways of compressing the data enough to make do with unexpected lower data rates, either as a matter of course, or under special situations when the chosen high-bandwidth service is not available or has slowed down significantly, because of technical problems. Or it is found to interfere with the direct and, or reflected GNSS signals that are the main data types.

So, to begin with and before going into more details, one could consider compressing the navigation receiver data using the navigation broadcast orbits and clock corrections for the GNSS satellites, transmitted by these in their respective navigation messages, and the

instantaneous orbit position, velocity as well as the receiver's clock correction of each CubeSat determined with its navigation receiver data.

However, real-time transmissions are only essential in the case when a CubeSat is overflying, for example some tsunami main waves, or the likely location of an earthquake or of a major volcanic eruption. Otherwise, data can be kept in the memory device of the receiver and downloaded to a ground station when flying within communication distance of it, in the usual way, while also uploading from it the necessary messages for the controlled operation of the CubeSats and the information useful to the operation of the receiver, such as a better ionospheric correction than the one in the navigation messages.

At a speed of some 7 km/s of the specular point and a length of a large tsunami of roughly between from 100 km to 200 km in the open sea where its detection and monitoring will take place, its main waves moving at a speed of 100 m/s - 200 m/s, a satellite will fly across it in less than a minute, or several times longer if it run along the wave before this curves away from the specular point straighter path, for a total of between less than one minute to a few minutes. Once the CubeSat leaves behind the tsunami, there might be other reflection points following it from new GNSS-R satellites also crossing the tsunami waves.

This will be possible when the CubeSat is at less than the maximum distance at which an event can be observed occurring in front or behind of its sub-satellite point, or some 2600 km away from this point along a maximum circle along the surface below. Altogether this adds up to the satellite gathering data on the tsunami waves heights over a distance of some 10,000 km, that at 7 km/s - 8 km/s, it will take almost twenty-five minutes per revolution, for total telephone communication charges, for example at the current usual IRIDIUM subscription rates, of $.60x20 = $12,00, not considering subscription or other charges. This could be more, or less, depending on the projected velocity of the waves along that of the satellite ground track.

Lossless compression of the GNSS navigation receiver data:

These data are needed to recalculate on the ground the position, velocity and clock error of the satellite already calculated on board with the navigation computer module of the navigation receiver, based on the received GNSS code delays and carrier phases as well as on the positions of the GNSS satellites and the corrections for their clock errors obtained from the various GNSS navigation messages. The reason for this recalculation will become clear in the next sub-section. The satellite could transmit to the ground its *navigation* receiver-obtained code, Doppler and phase data (as to be explained, these can be compressed losslessly), as well as its approximate position, velocity and clock error obtained on board from such data with this receiver's built-in computer. Compressing for transmission the position, and for the first time the velocity etc. and also the code, phase and Doppler data can be made with a numerical-differences algorithm such as Hatanaka's [2], widely used to compress low-noise GNSS data, including those from a number of NASA's LEO missions. Before being distributed, the data is usually further compressed with a commonly available lossless method, for example with tools such as Linux's "gzip."

The use of Hatanaka's technique can fail when the data are seriously corrupted and it is necessary to re-start the procedure, something not always reliably detected with the usual dedicated

computer software, so some automated assistance on board, including from e.g. an appropriate neural-network algorithm, might be used to this end.

A different method from Hatanaka's is described next for losslessly compressing the noisy GNSS-R receiver code, phase and Doppler data. It begins by subtracting from each measurement of the received code, phase and Doppler the equivalent distance, phase difference and relative velocity between the GNSS satellite and the CubeSat, based on the known orbits of the GNSS satellites as provided by the navigation messages of each GNSS and the corresponding position and velocity values for the CubeSat obtained on board. To also know on the ground the instantaneous position and velocity of the CubeSat as calculated and used on board, their six vector-components could be transmitted, if needed, from the CubeSat compressed with a numerical-differencing method such as Hatanaka's followed by another lossless procedure, such a "gzip" and transmitted along with all the other receiver data.

Lossless compression of the code delay data (also known as pseudorange).

After the correction outlined at the end of the previous paragraph, one result is a residual code equal, at any of the chosen signal carrier frequencies, to the effect of the ionosphere on the signal at this frequency plus the noise in the code at this frequency. At the altitude of the satellites, the ionospheric effect will be a few meters, much less than at ground level, because the ionosphere normally has its maximum free-electron density at considerably lower altitudes than the 550 km - 600 km of the satellites. (For what this ionospheric effect is like and how to correct it as part of compressing the data, see the Appendix.) The data noise in the code should be also of at most a few meters.

So the transmission time delay, or code-data, multiplied by the speed of light to obtain the instantaneous distance between a GNSS satellite and the CubeSat, usually more than 20,000 km, can been reduced to a few meters or, equivalently, a few tens of nanoseconds, after subtracting that product from the data. All these operations can be reversed on the ground, where all that is needed to find out what was done to compress the code data in the CubeSat becomes known from the received transmissions, so it can be calculated precisely and removed from the compressed data to decompress it.

Lossless compression of the carrier phase data:

As to the carrier phase data, a procedure somewhat similar to that used for the code can be employed:

1) Convert the receiver-measured phase difference between CubeSat Navigation receiver and GNSS transmitter to a distance by multiplying this phase by the wavelength of its signal-carrier in vacuum, and subtract from this their already determined mutual distance using their calculated positions leaving in the result their errors, both of a few meters, as well as the ionospheric effect on the phase, plus the receiver's phase thermal data error and phase multipath, these two, in total, usually one or two cm (so they can be ignored for now), plus a phase ambiguity equal to an unknown integer number of cycles, or of corresponding wavelengths.

2) Round off the residual phase obtained as above to the closest number of integer cycles (expressed as wavelengths) and subtract this from this residual. That should reduce the residual phase data to at most one half-cycle, or half wavelength. The wavelength for the carrier frequencies being around 20 - 25 cm, so its half is some 10 - 12.5 cm, the transmission of this remaining half-cycle at one-millimeter level (the usual level, at present, of a GNSS receiver thermal noise, to avoid adding a significant quantizing error) will require 8 bits per frequency, including the sign bit, or 16 bits (2 bytes) for the two frequencies.

The number of cycles used to compress the phase data should be kept constant from the moment when this number is determined and starts to be applied, unless some big and instantaneous change in it happens; if so the new value should be applied. When other, small changes in the ambiguity happen due to partial losses of signal lock known as cycle slips, the value of the residual phase will change by one cycle or more. When, after a while, the cumulative change becomes larger than some chosen threshold, the subtracted ambiguity should be changed to a new value to return the residual phase to being equal to +/- half a cycle.
Every time the ambiguity correction is changed, a flag usually equal to 0 should be set to 1 in a flags' section at the end of each epoch of data transmission. The likely cycle-slip value, if found at the satellite, may also be included in the transmission. The actual cycle slip corrections should be found and applied on the ground using the same information better, with greater computing power and taking those flags and values into account, but not exclusively.
As previously mentioned, following this compression, a second, standard lossless one such as "gzip" can be used to further reduce the number of bytes to be transmitted to a more manageable level.

The exactly opposite process used to compress the phase can be followed on the ground to decompress it, except that this will leave behind the original number of ambiguity cycles plus the ones used to finish compressing the phase. However, this sum is just a different ambiguity from the original one and can be estimated and corrected using the same time-tested procedures ("floating" or "fixing" the ambiguity) that would have been used to remove the original ambiguity.

As a result of this compression, the code and phase data would have been reduced to the error in the two satellite positions along their line of sight, as determined with the CubeSat navigation receiver's computer from these very data and from the Navigation Message, plus the ionospheric effect and, in the case of the phase, the modified ambiguity. This would be altogether of a few meters, and so some millions of times smaller than the original measurements. After the data are decompressed, following the opposite procedures used to compress them and in reverse order, the position errors of the satellites, etc. can be removed when fully processing the data using, for example, very precise dynamic orbit estimation procedures as implemented for example in "GEODYN", the NASA Goddard Space Flight Center's Geodesy and Geophysics Laboratory's main operational software for precise orbit determination, fundamental reference frame realization, and gravity field modeling of Earth and other planetary bodies. As to the modified ambiguities in the a priori phase residuals, this can be estimated and removed using standard

methods. Cycle slips can be found and corrected using also well-known and well-tested procedures.

Lossless compression of the reflectometric receiver data:

As to the Doppler compression, so far not discussed, more is said in the second paragraph of this sub-section about both the Navigation and the reflectometric receiver's Doppler data.

To some extent, the compression procedure used for the GNSS navigation receiver data can be used for the reflectometric receiver as well, replacing the straight line-of-sight distance between CubeSat and GNSS satellite with that along the shortest path (already considered) of the reflected signal: in straight line from GNSS satellite to specular point; in another straight line from specular point to CubeSat. An approximate value of the ionospheric effect must be removed from this shortest path according to an ionospheric model that can be used to make an approximate correction of the total free electron content along the reflected signals, each of which passes once through the upper and twice through the lower ionosphere, from the GNSS satellite to the specular point to the CubeSat. This could be equivalent to adding several tens of meters to the direct signal's ionospheric effect, because of the denser lower ionosphere crossed twice, perhaps at shallow angles.

To deal effectively with the greater distance travelled by the reflected signals and also with the larger ionospheric effect would require two additional things:

(1) The calculation of the position of the specular point, something for which there are well-established procedures and should be one of the computations made in the CubeSat computer.

(2) Estimating the ionospheric effect by subtracting from each other two codes, one for each of two carrier frequencies chosen (with GPS, for example, these would be C1C in the L1 band with C2C, or CW2, and with CW5 in the L2 and L5 bands, respectively), as well as correcting each code for the transmitter internal line delay and for that in the receiver, the latter to the extent that it can be calibrated on the ground using the downloaded compressed GNSS-R receiver data (the transmitter's delay is included in the navigation message). The result, with the two-code difference multiplied by a function of the squares of both frequencies and by a scale constant, is now a noisy estimate of the total electron content along the total path of the reflected signals. This can be used, in turn, to correct the ionospheric effect on the code and phase of each of the chosen two frequencies by diving this just obtained total electron content by the square of the corresponding frequency. Only one ionospheric electron content value per GNSS whose signals the receiver has locked on, that of the difference of the codes of the two frequencies chosen, is needed to compress in this way, before transmission from the CubeSat, and also after ground reception, decompress both the code and the phase data. However, when applying it, this correction should be subtracted from each code but added to each phase. One thing not used here is something like Hatanaka compression, as the data noise is too rugged for this approach to work reliably, given the much weaker signal to noise ratio than in the case of the Navigation receiver data.

Lossless compression of the Doppler data:

The following applies in part to both the Doppler obtained with the Navigation and with the reflectometric receivers:

This procedure follows similar lines as the code compression one, but in this case using, as calculated with the on-board navigation computer, the Doppler in the straight line from the specular point to the Cubesat minus that from the GNSS satellite to the specular point. Each Doppler being the projection of: (1) the known velocity of the GNSS satellite (from the navigation message orbit parameters) in the direction of the specular point, and (2) that of the CubeSat velocity (from the receiver computer's navigation solution) in the direction from the specular point to the CubeSat. At this point, the Navigation receiver Doppler can be compressed reliably and further using the Hatanaka method, but not the noisier GNSS-R Doppler and ending with a third form of lossless compression, such as with Linux's "gzip."

In the case of the noisier GNSS-R data, the Doppler cannot be compressed with Hatanaka's method. The subtraction of the calculated Doppler from the actual measured one is followed, instead, by a Doppler ionospheric correction, made similarly as the one for the code by using, in this case, instead of the difference of the two codes, that of the two GNSS-R measured Doppler shifts, one for each of the frequencies chosen, as already explained. This is to be followed, once more, by a second lossless compression with, for example, "gzip."

Delay Doppler Maps:

If the effort to detect the presence and determine the main characteristics of a tsunami (position, velocity, direction and wave length) could be helped using DDMs, as some have proposed (see reference [3] in the tsunami detection section), unlike its offline processing for studies based on the signals of Global Climate (see section (6) on this topic), the transmission of some of these maps to the ground might have to be made in real time as well. The maps can be data-heavy and have correspondingly large numbers of bits to be transmitted. The number of bits needed to describe a DDM is the product of three numbers, each of which is larger for a finer resolution of the map and a better picture of what it represents:

1) The number of Doppler Delays.
2) The number of Doppler shifts.
3) The number of levels of correlation power used at each Doppler/Delay coordinate pair.

For example, for 20 Doppler shifts and 20 delays, arranged in a 20x20 square grid of cells or pixels with sixteen levels of correlation power or "colors" each, the number of bits would be 20x20x4 = 1,600 bits, or 200 bytes. But those bits of power level are the only ones that need to be transmitted, as assumed in this calculation of the bits. They can be transmitted in a predetermined and known order, for example starting from the leftmost and uppermost grid cell and proceeding from left to right, lower row after lower row, until completing the transmission at the rightmost one of the bottom row. Doubling, for example, the resolution of any of these three coordinates will double the number of bits to be transmitted.

Because to design the transmission message it is necessary to consider first the number of bits per DDM, the product of its chosen number of columns, rows, and levels of correlation power, the total bits to be transmitted by each CubeSat is to be found, conservatively, by multiplying that number by the planned maximum number of satellites of any GNSS simultaneously tracked with a CubeSat receiver and then multiplying this by the planned number of GNSS systems to be tracked simultaneously with this receiver. Clearly, the number of bits transmitted by each CubeSat can become high very quickly with an increasing resolution of the DDM.

There may be ways of compress these data, but probably not both as straightforward or lossless as in the case of the receiver data considered in the previous paragraph. So one way out of this dilemma would be to use the Certus 700 service, with a bandwidth of 704 Kb/s.

However, if one could also see first each DDM to decide if it may be useful enough to deserve to be transmitted, then one could select for transmission only those likely to be of any use. Since one is unlikely to be doing this inside a CubeSat, an alternative could well be the use of a neural network of appropriate design, trained to recognize DDMs likely to be useful, and let those be transmitted in real time, leaving the rest to be sent to ground stations during regular data dumps. This neural network could be run in a dedicated chip, or set of chips of appropriate design, such as GPUs and other fast and commercially available integrated circuits.

References:

[1] Murbach, M. et al.; Use of Iridium as a Primary Encrypted Command/Control Gateway, in Topics in Advanced Communication and Design in the TES-n Nanosatellite Flight Series, S3VI Webinar; March 18, 2020.

[2] Hatanaka Y., A Compression Format and Tools for GNSS Observation Data, Bulletin of the Geographical Survey Institute, Vol.55 March, 2008.

8) The Possible Uses of Spire GNSS-R Data.

Grazing Angle GNSS-R Altimetry from the Spire satellite constellation

Through NASA's Commercial Smallsat Data Acquisition Program (CSDA), Spire has produced a grazing angle GNSS reflectometry product for altimetry applications with a roughly 30-day latency. This product is quasi-global but focuses on certain regions of the global including the Arctic, Antarctic, and Southeast Asia. Spire's current constellation provides GNSS-R observations from a couple dozen low earth orbiting CubeSats tracking dual-frequency GNSS satellite signals. We have sampled this data for dates in 2022 to better understand the coverage and quality of GNSS-R measurements as collected on a real-world smallsat constellation in low earth orbit. Here we present a preliminary summary of our findings.

Spire Product Description

Through the CSDA online platform, Spire provides track-by-track NetCDF files containing grazing angle GNSS-R altimetry measurements and metadata, called the "Spire Level-2 Grazing Angle GNSS-R Altimetry" product. A similar product is also provided for Sea Ice, which may be of interested to other applications beyond tsunami detection and tracking. Additionally, Spire provides products measuring radio occultations (RO) and RO excess phase, near-nadir GNSS-R, ocean wind derived from GNSS-R bistatic radar, attitude and navigation files, and more.

The GNSS-R Altimetry product files include measurement and location information for each observation including height, mean sea surface, latitude, longitude, angle of elevation, slant bias, distance to coast, atmospheric delay, ocean tide model, and total unwrapped phase for reflected and direct L1 and L2 GNSS signals. This choice of file type means that numerous open-source packages can be used to study this data; in our preliminary look, we used Python's pandas and xarray packages to examine data and used the matplotlib and cartopy packages to visualize that data. A more complete description of the Spire Level-2 Grazing Angle GNSS-R Altimetry product can be found at: https://spire.com/federal/nasa/nasa-csda-program-product-summaries/.

Example coverage for July 1, 2022 is shown globally in Figures 18 and 19. To date, Spire has focused their GNSS-R processing primarily in the Arctic, Antarctic, and Southeast Asia, and subplots focused on each region are provided in the figures. Figure 18 shows GNSS-R tracks recovered by each Spire low earth orbiting satellite (named FM###). Figure 19 shows computed sea level anomaly relative to the DTU18 mean sea surface and ocean tides extracted from the TPX09-atlas v1 ocean tide model (provided as part of the GNSS-R dataset by Spire). For more in-depth scientific study, efforts would need to be made in verifying proper handling of tides as well as long-term sea level changes.

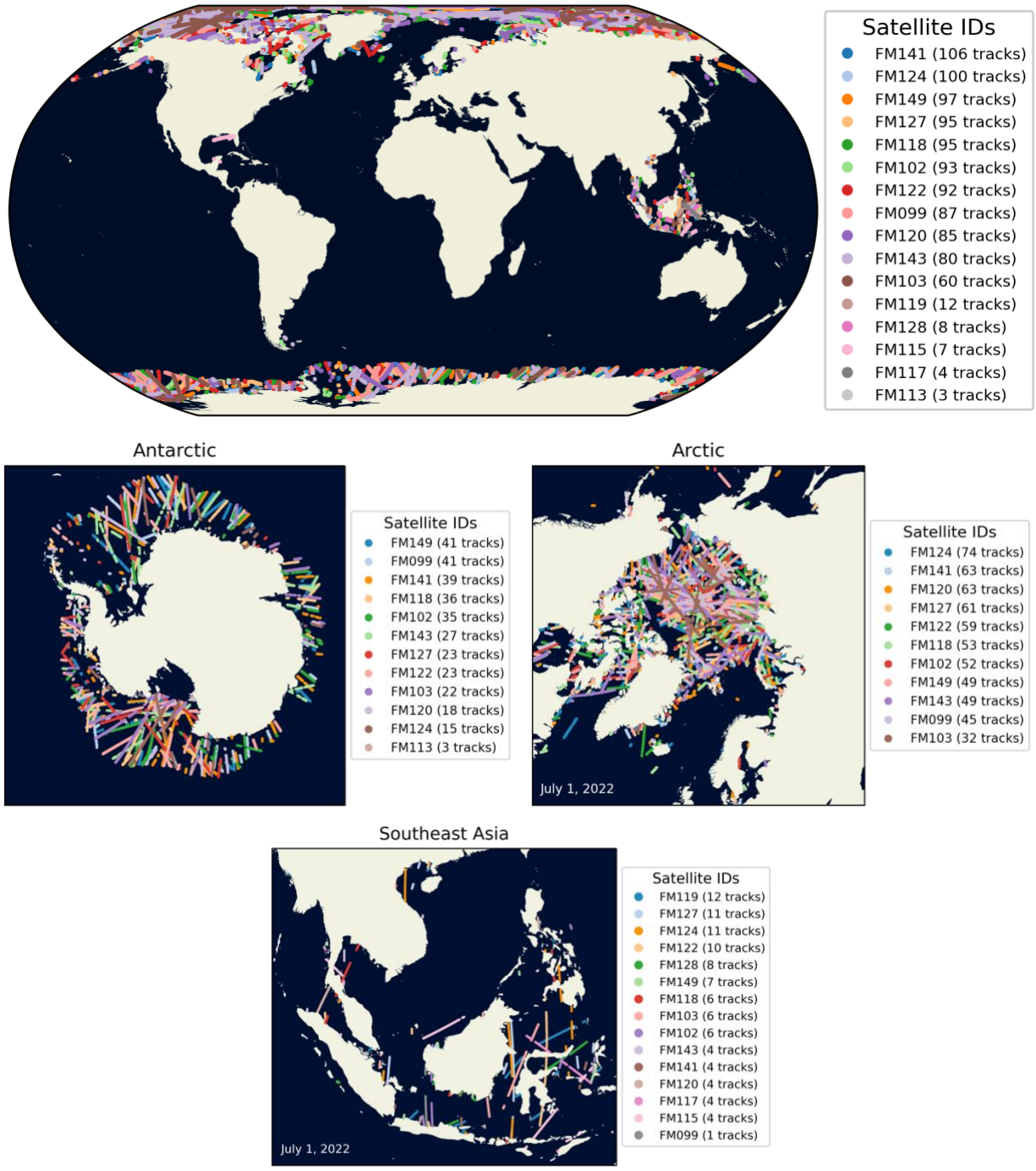

Figure 18: GNSS-R reflections measured by Spire constellation on July 1, 2022, per each Low Earth Orbit satellite "Flight Module", denoted by FM### (source: Spire Level-2 Grazing Angle GNSS-R Altimetry Product). A global map is shown along with three zoomed-in local projections.

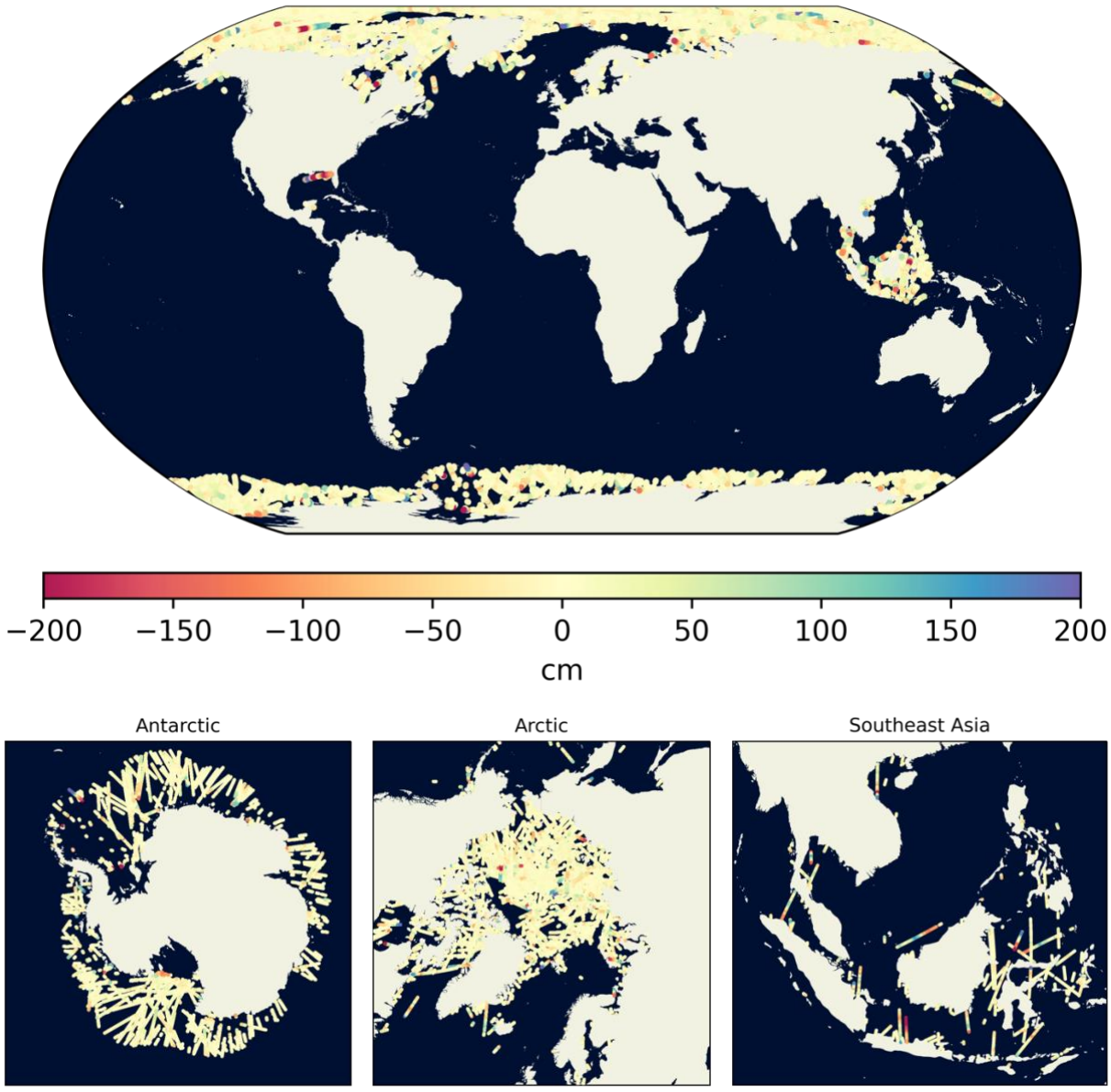

Figure 19: Sea Level Anomaly measurements relative to DTU18 mean sea level + an ocean tide model for July 1, 2022 (source: Spire Level-2 Grazing Angle GNSS-R Altimetry Product). Global measurements between -2 and 2 meters are shown in the top plot. Spire's GNSS-R product focuses on the Antarctic, Arctic, and Southeast Asia, enlarged in the plots in the second row.

Coverage Statistics

To better understand the average data availability with the current Spire constellation, and therefore be able to translate that availability to a theoretical larger future constellation, we examined the Southeast Asia region over the month of January 2022. Over the course of that month, we found an average of 133 GNSS-R tracks per day (min 97, max 167) with an average track length of 205 km (min <1 km, max 2208 km). The average track contained approximately 1475 individual reflections. Reflections were detected by an average of 20 low earth orbiting satellites per day (min 17, max 23). Figure 20 shows the average daily tracks observed over Southeast Asia, binned in 5-degree x 5-degree latitude/longitude blocks. The primary focus area around the islands in the region shows an average of 5-15 reflection tracks per day. This number could be expected to scale directly with a larger low earth orbiting satellite constellation.

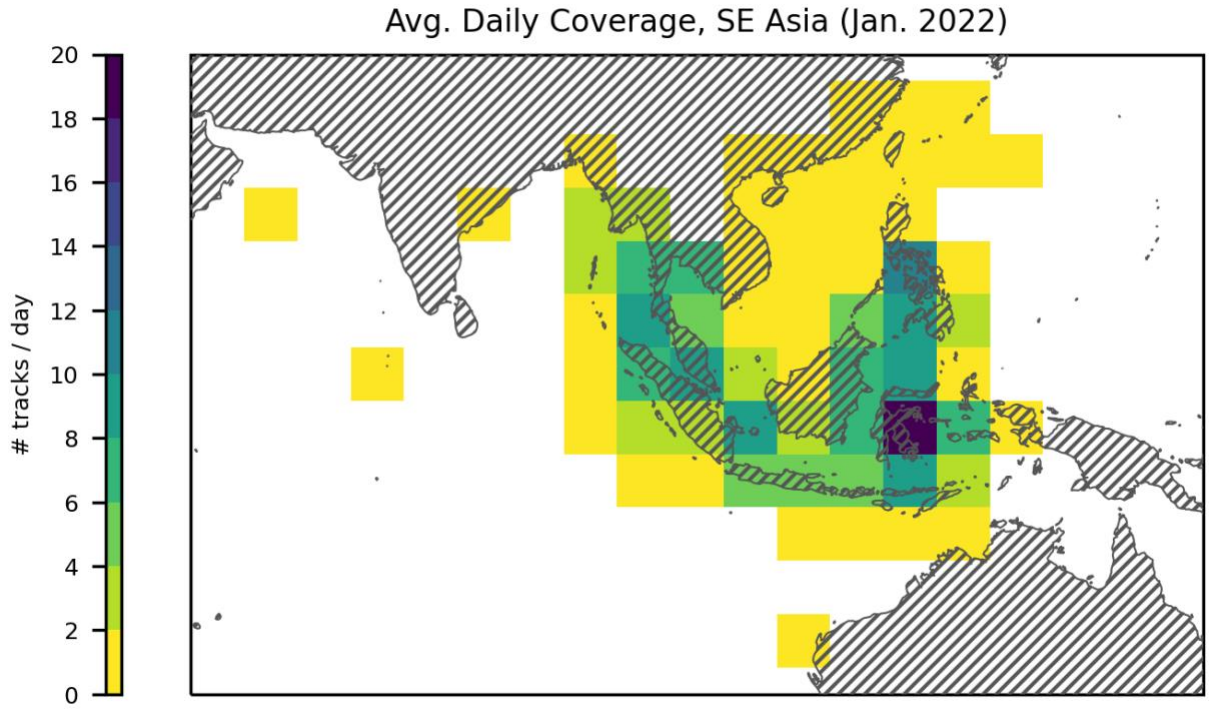

Figure 20: Average daily number of Spire GNSS-R tracks across 5-degree x 5-degree blocks in Southeast Asia during January 2022. Similar coverage could be expected in other like regions.

Additionally, we examined the distributions of sea level anomaly measurements track statistics. Figure 21 shows a histogram of sea level anomaly measurements for January 2022, as well as cumulative distribution functions of both the RMS of sea level anomaly measurements per reflection tracks and the length (in kilometers) of those reflection tracks. 75% of tracks show an RMS of less than 46 cm and cover a distance between 0 and 272 km, while less than 10% of tracks coverage a distance longer than 500 km and only 2% of tracks are longer than 1000 km.

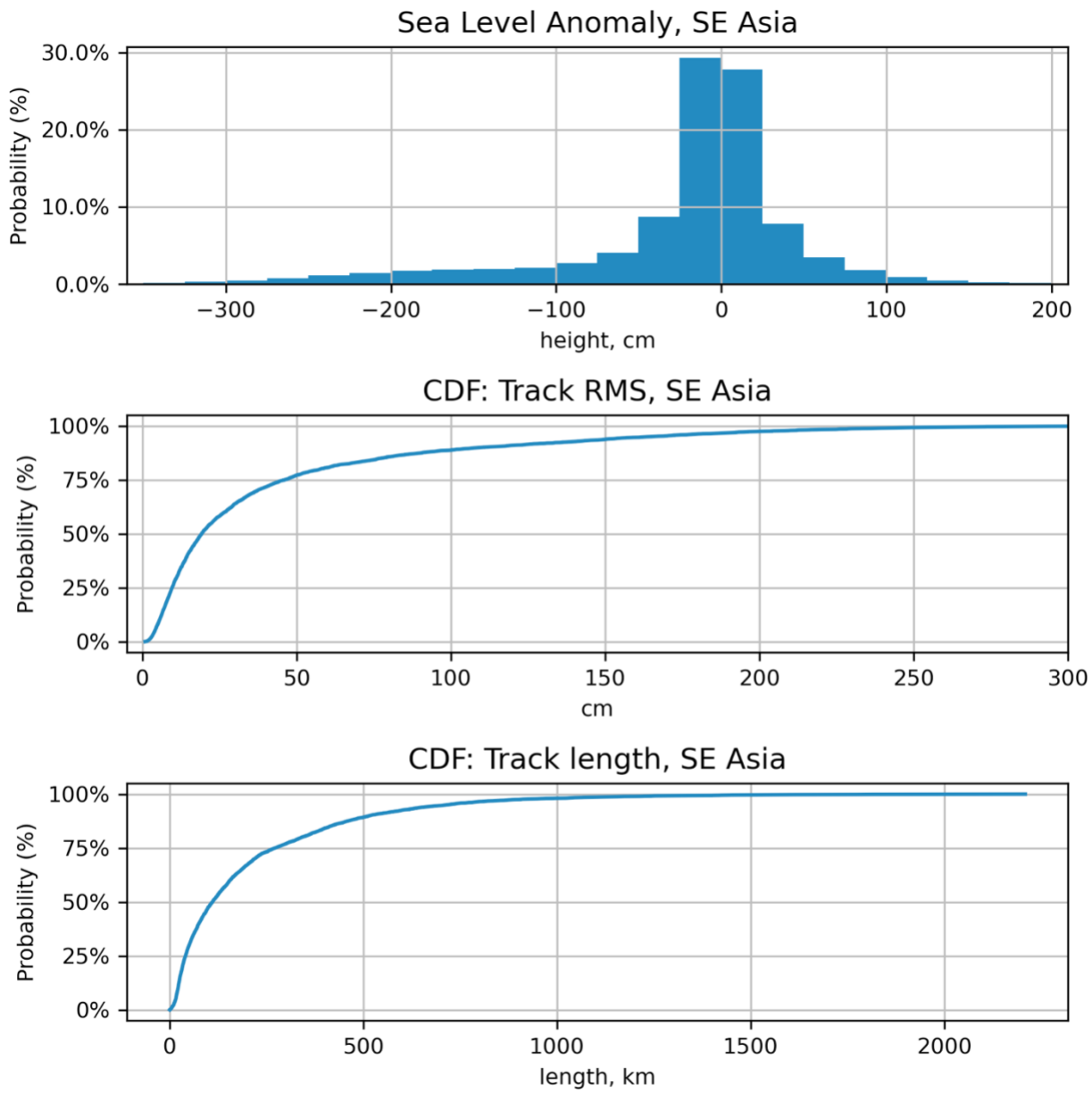

Figure 21: Coverage statistics from Spire GNSS-R measurements in SE Asia for January 2022: (top) histogram of sea level anomaly measurements relative to DTU18 mean sea surface; (middle) cumulative distribution function of the RMS of sea level anomaly measurements along each GNSS-R track; (bottom) cumulative distribution function of the length of each observed GNSS-R track.

9) Issues to Investigate Further, Some Using Simulations.

Given future funding to this effort, additional time should be dedicated to:

a) Working out in more detail and greater depth some of the topics mentioned in this report, such as the diverse uses of GNSS-R remote-sensing for monitoring climate change. Investigating further also its use for detecting and predicting the path of tsunami in spite of the often noisy GNSS-R data, as suggested by the results of investigating the properties of today's GNSS-R data in Section 8. Taking advantage for this of the unique characteristics of tsunami: wavelengths of hundreds of km, speeds of 100 to 200 m/s and maintaining their shape for considerable periods of time. This study may also include how to start and update hydrodynamic models using the GNSS-R data from many CubeSats to make the most precise predictions possible, using a form of Bayesian recursive estimation such as the Ensemble Kalman Filter. It is also precise to study ways of correcting GNSS-R data for tropospheric "wet" and "dry" GNSS signals' refraction along the fast-moving specular points tracks. Same observations can be made about extracting from the data the signatures of big, explosive eruptions and earthquakes in the ionosphere.

b) In more detail: Investigate and test the use of hydrodynamical models for refining the estimates obtained, in a preliminary step, using published techniques to analyze GNSS-R signals reflected from tracks of specular points passing across tsunami waves, to get initial estimates of their shape, direction, and speed. These models could be started using those estimates and then updated more or less continuously and in near-real time with additional Navigation and reflectometric data, in a global analysis. Such as one based on a state-space representation of the ocean's hydrodynamic model, using an appropriate recursive Bayesian estimation procedure such us the Ensemble Kalman Filter.

(c) A similar approach using dynamic (physics-based) ionospheric models can be used to create a time-dependent, 3-D global ionospheric map using the free-electron content data obtained with Navigation and GNSS-R receivers by combining direct and reflected signals of different frequencies. This problem differs in the characteristics of the signals of interest to be detected and mapped in time and space from those in the oceans, but the size of the state space is also very large. So this topic also should be addressed in a further study of how to use GNSS-R data to adjust and steer oceanic and ionospheric models as dynamic systems with very large state spaces.

d) Simulating data to be used, among other things, in covariance error analyses, to study possible ways of processing the data that may be obtained continuously from an assumed constellation such as the one described in Section 1, with eight distinct high-inclination orbit planes and as many as 45 CubeSats in each plane, all in near-circular, high-inclination orbits with a height of between 550 and 600km. Time allowing, investigate in this way the likely results assuming other constellation arrangements, particularly with different numbers of satellites per plane.

e) Investigate the possible computer power that might become available in the near future for use in CubeSats to make more calculation on board, including some very powerful small processors now being developed.

f) Look for a desirable set of CubeSat compatible hardware components and see, i detail, what are the choices currently available. And also try to find out what they might be like in the not too distant future based on work now under way towards improving hardware.

g) Make an in-depth study of the Spire GNSS-R data and its derived products available through their deal with NASA, to gain a necessary understanding how all this could be done in a future mission. This as part of a steadily funded project, with a group of experts assigned to work on it.

h) Process samples of actual GNSS and GNSS-R data of the kind suitable for eventual use in a mission like the one described in this report; processing these data with software owned by NASA, or developed in-house, as well as borrowed from elsewhere in order to get a direct feeling for some of the main practical issues involved.
Obtain also some products of such data (e.g. showing the quality and extent of sea ice cover) such as those that might be provided by Spire to NASA, to compare with and so validate the results obtained at NASA using the same data.

i) Writing, for publication, as appropriate, papers on the various aspects of this idea of a mission, illustrated with some results obtained off-line with real data.

j) A final, comprehensive report on all the work done, the results obtained and consequent conclusions.

10) Summary and Conclusions.

This study has concentrated, guided by previous knowledge, ideas read in the published literature, as well as conversations with experts on relevant subjects, on exploring the possible detection and tracking in near-real time of tsunami using the type of CubeSat constellation described in this report, with each CubeSat equipped with a GNSS-R receiver as the main sensor, as well as for the detection and evaluation of earthquakes and volcanic eruptions. The ultimate goal being to ensure the issuing of advanced warnings of approaching tsunami to communities at risk and help this way to save lives. As well as, in the aftermath of any of these three types of often disastrous events, help those regional authorities in charge of responding to the situation to evaluate quickly and correctly the magnitude of the likely material damages and the probable number of homeless, injured, disappeared and dead, to help prepare and deliver a response adequate to the likely magnitude of the catastrophe.

A secondary goal of this initial project, has been to understand the best way to use the same constellation to observe various kinds of large changes on the Earth's surface and atmosphere indicative of the extent, seriousness, rate and sense of Global Climate Change. The expectation of getting sufficiently good results with GNSS-R techniques even as these are today, is based on the existence of a large body of published work on using GNSS-R data to study facts relevant to Global Climate Change from missions such as NASA's pioneering one, CYGNSS. One important consideration to keep in mind is that, given that private companies are providing data and analysis of such data to ends that overlap with those of the proposed mission, the data collected during the proposed mission by NASA should be used in collaboration and not in competition with private enterprise.

The conclusions, so far, are these:

A constellation of CubeSats equally distributed, perhaps with as many of 45 satellites in each of eight high inclination orbit planes with regularly spaced ascending nodes, the CubeSats equally spaced in each plane along a common, near-circular high-inclination orbit at an altitude of some 550 - 600 km, can provide a dense GNSS-R coverage of almost the whole world at each single orbital revolution of about 96 minutes duration.

The data from the satellites when no tsunami, earthquake, etc. is happening can be downloaded as usual, by transmitting the data, along with telemetry and other information to be used off-line, to ground stations as each CubeSat passes close enough to one of them. However, when one of those major natural hazards is known to be underway, the data should be compressed further to be transmitted both soon and fast enough to be used in near-real time, and for that to be possible communication needs to be made and maintained using reliable channels likely to be available without delays and with sufficient bandwidth. A preliminary investigation suggests that some of the satellite-based telephony services available today, for example those of the Iridium company that owns the equally named low-orbit satcom constellation, may be adequate for this purpose, and also that the necessary equipment can be small and low-power enough to be used in CubeSats.

The deployment of the constellation of CubeSats, its operation and maintenance as well as the use of the data as intended, probably would be the outcome of an international cooperative effort also involving private and public partnerships with companies already operating small, independent CubeSat constellations for related purposes and, or processing the collected data to this end.

Finally: of future studies in the areas already considered, data analysis should be a major component, some of it involving substantial quantities of real GNSSS-R data as well as ever more realistic simulations, would have to be made in a scale proportionate to the resources and numbers of skilled personnel available.

The mid-term goal is to fly a smaller demonstration mission, or else partner with a third party to acquire data from CubeSats built to the required specifications by outside vendors and contractors (e.g., through NASA's CSDA program), as a proof of concept for an eventual full mission.

Acknowledgements:

We thank Jeanne Sauber for generously helping us improve this document by reading and commenting on it. Funding for this study was provided by the NASA GSFC Internal Research and Development (IRAD) Program FY22, proposal number 246.

Appendix on the Ionospheric Effect and its Correction.

The basic observation equations for GNSS are:

For the code, also known as pseudorange:

$$P_{Li} = \rho + c(dt_r - dt_s) + T + \alpha_f STEC + K_{p,r} - K_{Ps} + M_p + \varepsilon_p \qquad (A1)$$

P_{Li} is the code with carrier frequency L_i (i =1, 2, 5 for GPS), **ρ** is the geometric range between the satellite and receiver antenna phase centers at emission and reception time, respectively (see article Geometric Range Modelling). Note: The Antenna Phase Centre (APC) is frequency dependent, but we neglect this effect here for simplicity (see article Antenna Phase Centre).

dt_r and **dt_s** are the receiver and satellite clock offsets from the GNSS time scale, including the relativistic satellite clock correction (see Clock Modelling).

T is the tropospheric delay, which is non-dispersive (see Tropospheric Delay).

α_fSTEC is a carrier frequency-dependent ionospheric delay term, where α_f is the conversion factor between the integrated electron density along the ray path STEC, and the signal delay at frequency f. That is, α_f=40.321016m signal delay (at frequency f)/TECU, where the frequency f is in Hz and 1TECU=10^{16}e−/m^2).

$K_{p,r}$ and **K_{Ps}** are the receiver and satellite instrumental code delays, which are dependent on the code modulation and carrier frequency.

M_p represents the effect of code multipath, also depending on the code and carrier frequency, and ε_P is the receiver noise.

As to the carrier phase:

$$\Phi_{Li} = \rho + c(dt_r - dt_s) + T - \alpha_f STEC + k_{L,r} - k_{Ls} + \lambda_L N_L + \lambda_{Lw} + m_L + \epsilon_L \quad (A2)$$

$k_{L,r}$ **k_{Ls}** are the phase delays in receiver and transmitter, **λ_{Lw}** is the phase windup and **m_L**, **e_L** are the phase multipath and receiver phase noise. NL is the number of ambiguity cycle in the phase.

(The Doppler is the time-derivate of carrier phase.)

The full expression for the code ionospheric delay (in m) is:

$$\text{delay} = 1/f^2 \; 40.308193 \int N \, dl \qquad (A3)$$

Here f, as before, is the carrier frequency of the signal (e.g. L_1, L_2, etc.) and the integral is along the line of sight from transmitter (GNSS) to receiver (CubeSat).

Calling the integral in the expression above S, then:

$$\text{delay} = 1/f^2 \; 40.308193 \; S \qquad (A4)$$

(The phase ionospheric delay is the same in modulus, but with opposite sign.)

S is usually referred to as the Slant Total Electron Content (STEC) inside a cylinder of 1 m^2 section and axis along the slanting line of sight from transmitter to receiver. It is measured in TEC units, or TECU. One TCU (already defined) is equivalent, at the frequency of L2, for example, to ~16 cm extra length compared to the geometric distance, or of ~0.5 nanoseconds of extra delay if divided by c. (*)

The above is the main effect of the ionosphere and the only term in the full mathematical expression of this effect large enough to be considered for the purpose of compressing the data as described in section (7).

There are two other terms of the ionosphere effect proportional to the cube and the fourth power of 1/f that are also functions of the magnetic field intensity. There is also a usually small second term also proportional to $1/f^2$ that causes a curvature of this path away from the perfectly straight line of sight from transmitter to receiver, or rather small except at low satellite elevations.
At very low elevations there is a significant downward curvature before, over and beyond the earth limb, as seen from a CubeSat, for example, due to a varying refraction index with height. And this curvature is what makes it possible to use of these bent signals to measure the refraction index along vertical columns of the atmosphere with the technique known as GNSS Radio Occultation, or GNSS-RO, using special GNSS receivers. From the refraction index and Doppler shift, it is possible to estimate the vertical profiles of the water-vapor content, temperature, and pressure in the lower atmosphere and of the free-electron content in the upper one. This has many applications: in meteorology, radio communications, space weather forecasting and monitoring, etc. and for such things as correcting GNSS data.

To find the required ionospheric correction for the code, one needs first to find the part that is not dependent on the frequency.
With two different signal carriers, for example GPS L_1 and L_2, calling this part C, one can write:

$$\text{delay}(L_2) - \text{delay}(L_1) = C/f_2^2 - C/f_1^2$$
$$= C(f_1^2 - f_2^2)/f_1^2 f_2^2 \qquad \text{(A5)}$$

So

$$(\text{delay}(L_2) - \text{delay}(L_1))\, f_1^2 f_2^2 / (f_1^2 - f_2^2) = C \qquad \text{(A6)}$$

Finally, the instantaneous ionospheric correction can be calculated by dividing C by f_1^2 or f_2^2, to correct the code at L_1 or L_2.
The same reasoning leads to the formulas for correcting the carrier, their only difference between those and the ones for the code being that the signs are opposite ones.

A different approach to largely eliminate the effect of the ionosphere is to the combine codes or phases and pseudoranges of two different carrier frequencies in what is known as the ionosphere-free combination of phase and code, respectively, where the first ionospheric term vanishes:

$$\Phi_{\text{iono-free}} = (f_1^2 \Phi L_1 - f_2^2 \Phi L_2)\,(f_1^2 - f_2^2)^{-1} \qquad \text{(A7)}$$
$$P_{\text{iono-free}} = (f_1^2 P1 - f_2^2 P2)\,(f_1^2 - f_2^2)^{-1} \qquad \text{(A8)}$$

(*) See the International Earth Rotation Service Conventions, 2nd Part of Chapter 9 -- with a very complete treatment of the ionospheric correction. he first Part of this chapter deals with the tropospheric refraction in the lower, neutral atmosphere.